iScience

CellPress
OPEN ACCESS

Article

Bacterial pore-forming toxin pneumolysin drives pathogenicity through host extracellular vesicles released during infection

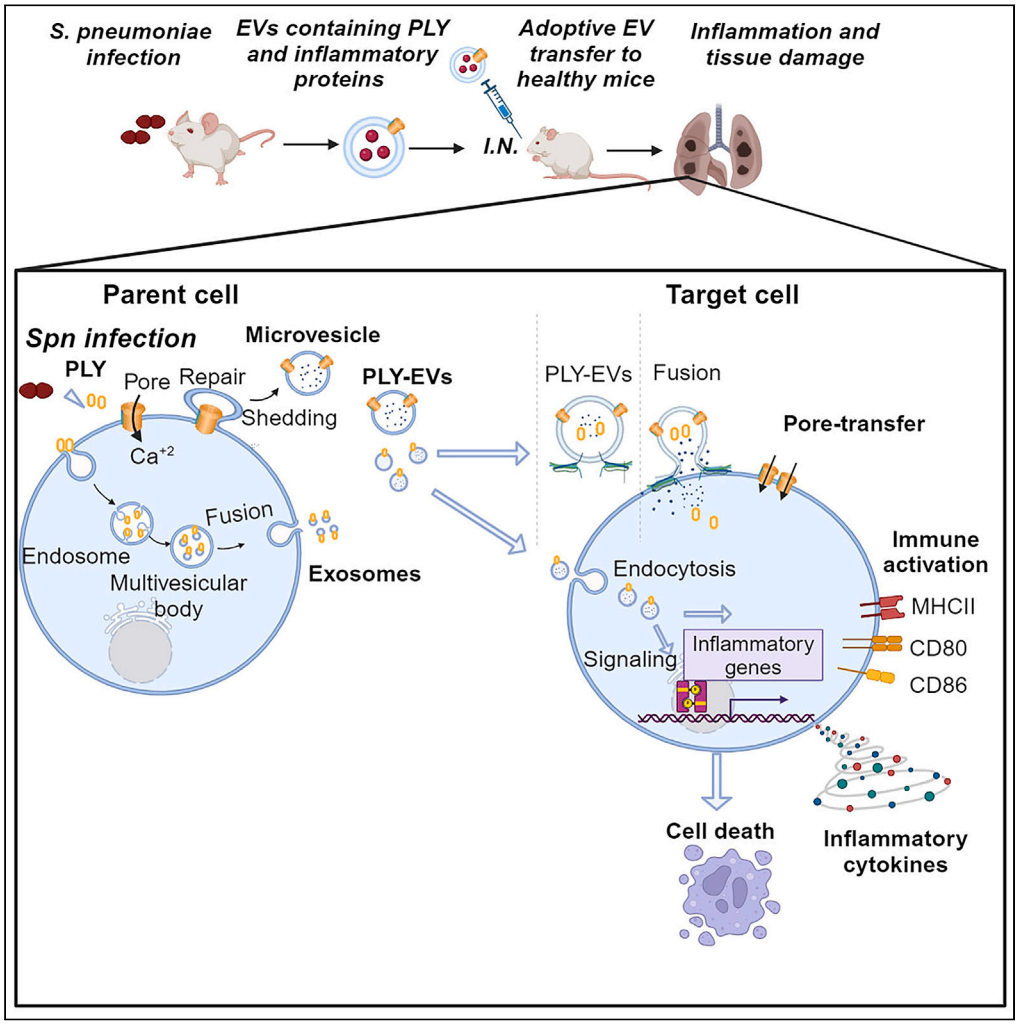

Saba Parveen, Chinmayi V. Bhat, Aswathy C. Sagilkumar, ..., Upendra Nongthomba, Anirban Banerjee, Karthik Subramanian

karthik@rgcb.res.in

Highlights

Bacterial cytotoxin, pneumolysin (PLY), upregulates shedding of host vesicles

Toxin transfer to recipient cells upon vesicle internalization induces cytotoxicity

PLY-induced vesicles are enriched for antimicrobial and inflammatory host proteins

Transfer of vesicles isolated from infected to healthy mice induces pathogenicity

Parveen et al., iScience 27, 110589
August 16, 2024 © 2024 The Author(s). Published by Elsevier Inc.
https://doi.org/10.1016/j.isci.2024.110589

iScience

CellPress
OPEN ACCESS

Article

Bacterial pore-forming toxin pneumolysin drives pathogenicity through host extracellular vesicles released during infection

Saba Parveen,[1,6] Chinmayi V. Bhat,[1,6] Aswathy C. Sagilkumar,[1,2] Shaheena Aziz,[1] J. Arya,[1] Asmita Dutta,[1] Somit Dutta,[3] Sautan Show,[3] Kuldeep Sharma,[4] Sumit Rakshit,[4] John Bernet Johnson,[5] Upendra Nongthomba,[3] Anirban Banerjee,[4] and Karthik Subramanian[1,2,7,*]

SUMMARY

***Streptococcus pneumoniae* is a global priority respiratory pathogen that kills over a million people annually. The pore-forming cytotoxin, pneumolysin (PLY) is a major virulence factor. Here, we found that recombinant PLY as well as wild-type pneumococcal strains, but not the isogenic PLY mutant, upregulated the shedding of extracellular vesicles (EVs) harboring membrane-bound toxin from human THP-1 monocytes. PLY-EVs induced cytotoxicity and hemolysis dose-dependently upon internalization by recipient monocyte-derived dendritic cells. Proteomics analysis revealed that PLY-EVs are selectively enriched in key inflammatory host proteins such as IFI16, NLRC4, PTX3, and MMP9. EVs shed from PLY-challenged or infected cells induced dendritic cell maturation and primed them to infection. *In vivo*, zebrafish administered with PLY-EVs showed pericardial edema and mortality. Adoptive transfer of bronchoalveolar-lavage-derived EVs from infected mice to healthy recipients induced lung damage and inflammation in a PLY-dependent manner. Our findings identify that host EVs released during infection mediate pneumococcal pathogenesis.**

INTRODUCTION

Streptococcus pneumoniae (the pneumococcus) causes human upper respiratory tract infections and kills over a million people worldwide annually.[1] Globally, *S. pneumoniae* is a major inducer of mortality due to pneumonia in children younger than 5 years[2,3] and the elderly older than 70 years. Recently, macrolide-resistant *S. pneumoniae* has been classified as medium priority among the top 15 pathogens that are most threatening to human health (World Health Organization, 2024). Pneumococcus colonizes the nasopharynx of 27%–65% of children and <10% of adults asymptomatically.[4] However, bacterial invasion into the lower respiratory tract and spread to internal organs leads to life-threatening diseases such as pneumonia, septicemia, and meningitis. Antibiotic misuse and horizontal transfer of antibiotic-resistance genes have led to the alarming spread of drug resistance among pneumococcal strains.[5] The existing pneumococcal polysaccharide and conjugate vaccines offer limited capsular serotype-dependent protection and have reduced the overall disease burden,[6] but the emergence of non-vaccine serotypes is a major problem worldwide.[7]

The pore-forming cytotoxin, pneumolysin (PLY), is a key virulence factor that plays a major role in colonization, invasion, and host-host transmission of the pneumococcus.[8–10] The binding of PLY monomers to cell membrane cholesterol triggers protein oligomerization into a 40- to 50-mer prepore structure, which collapses vertically to form β-barrel pores of 30–50 nm in host cells.[11–13] Pore formation induces calcium influx into the cell, leading to membrane instability, osmotic imbalance, and eventually cell death. However, at sublytic doses of PLY, calcium-dependent membrane repair processes avert cell lysis by plugging the PLY-induced pores and eliminating the membrane pores as microvesicles.[14,15] Both microvesicle shedding and endocytosis contribute to removal of PLY pores from the damaged cell membrane.[16–18] Extracellular vesicles (EVs) are classified into three major types, namely, exosomes (30–200 nm), microvesicles (100–1,000 nm), and apoptotic bodies (>1,000 nm), based on the size and biogenesis mechanisms.[19,20] Exosomes are endocytic in origin and are released when the intraluminal vesicles of the endosome fuse with the plasma membrane. This is primarily mediated by the endosomal complex required for transport (ESCRT) proteins and Rab GTPases.[21] Microvesicles are relatively heterogeneous population of vesicles, which are generated by direct

[1]Host-Pathogen Laboratory, Pathogen Biology Division, Rajiv Gandhi Centre for Biotechnology, Thiruvananthapuram 695014, India
[2]Regional Centre for Biotechnology, Faridabad 121001, India
[3]Department of Developmental Biology and Genetics, Indian Institute of Science, Bangalore 560012, India
[4]Bacterial Pathogenesis Laboratory, Department of Biosciences and Bioengineering, Indian Institute of Technology Bombay, Mumbai 400076, India
[5]Virology Laboratory, Pathogen Biology Division, Rajiv Gandhi Centre for Biotechnology, Thiruvananthapuram 695014, India
[6]These authors contributed equally
[7]Lead contact
*Correspondence: karthik@rgcb.res.in
https://doi.org/10.1016/j.isci.2024.110589

This is an open access article under the CC BY-NC-ND license (http://creativecommons.org/licenses/by-nc-nd/4.0/).

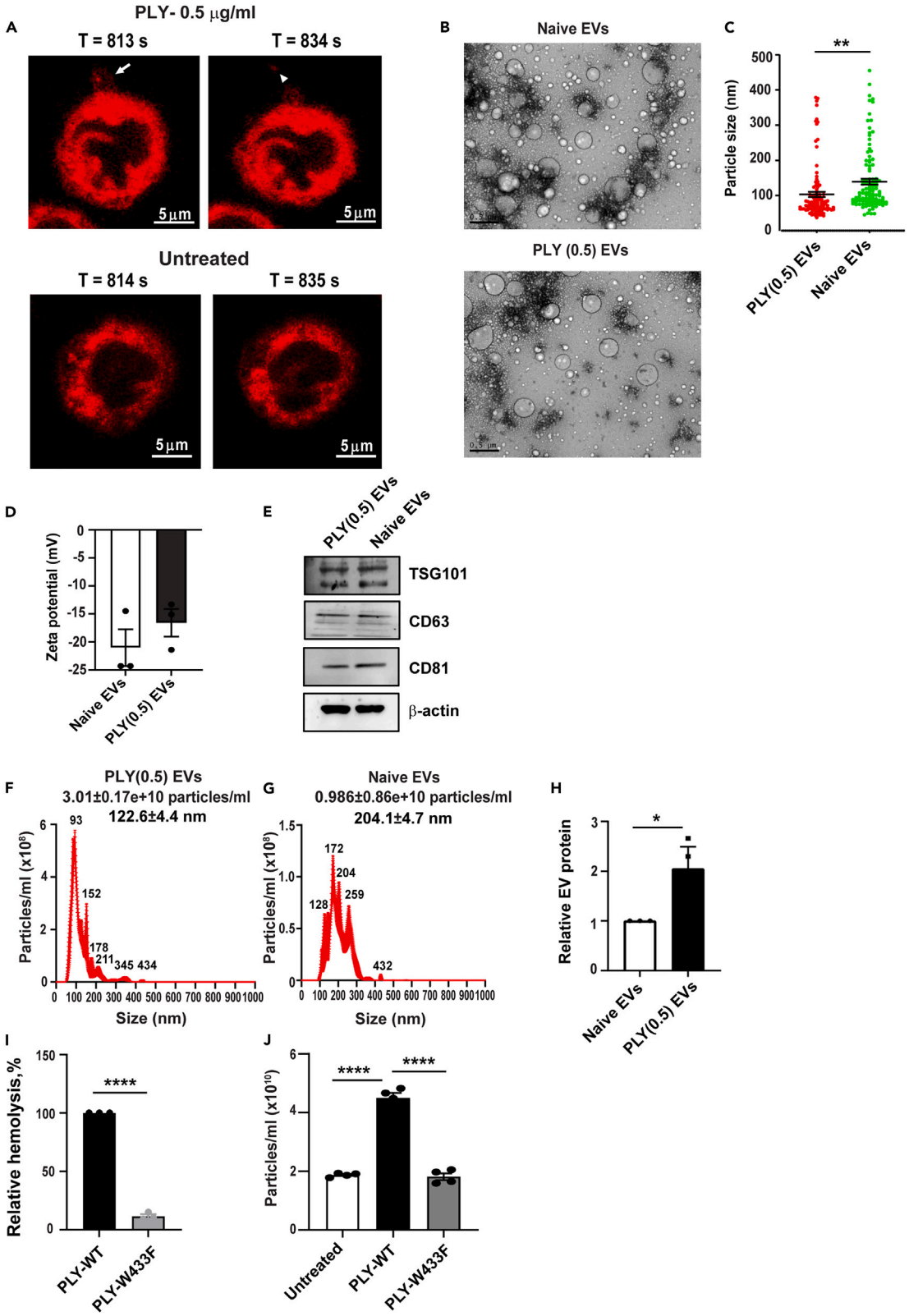
A
PLY- 0.5 μg/ml
T = 813 s
T = 834 s
5μm
5μm
Untreated
T = 814 s
T = 835 s
5μm
5μm
B
Naive EVs
PLY (0.5) EVs
C
**
Particle size (nm)
500
400
300
200
100
0
PLY(0.5) EVs
Naive EVs
D
Zeta potential (mV)
0
-5
-10
-15
-20
-25
Naive EVs
PLY(0.5) EVs
E
PLY(0.5) EVs
Naive EVs
TSG101
CD63
CD81
β-actin
F
PLY(0.5) EVs
3.01±0.17e+10 particles/ml
122.6±4.4 nm
Particles/ml (x10⁸)
93
152
178
211
345
434
Size (nm)
G
Naive EVs
0.986±0.86e+10 particles/ml
204.1±4.7 nm
Particles/ml (x10⁸)
172
204
259
128
432
Size (nm)
H
*
Relative EV protein
Naive EVs
PLY(0.5) EVs
I
****
Relative hemolysis,%
PLY-WT
PLY-W433F
J
****
****
Particles/ml (x10¹⁰)
Untreated
PLY-WT
PLY-W433F

Figure 1. Pneumolysin (PLY) enhances shedding of extracellular vesicles from monocytes at sublytic doses

(A) Snapshots of selected time frames from live imaging of Nile-red-labeled human THP-1 monocytes challenged with recombinant PLY (0.5 μg/mL). Arrow indicates membrane protrusions (T = 813s), and arrowhead points to the subsequent EV release (T = 834s). Scale bars, 5 μm.

(B) Transmission electron micrographs (N = 3) of EVs isolated from PLY-challenged (PLY-EVs) and untreated cells (naive EVs). Scale bars, 0.5 μm.

(C) Quantification of EV particle size from TEM images showing significant smaller size of PLY-EVs compared to naive EVs. $^{**}p < 0.01$ by unpaired t test.

(D) Zeta potential (ZP) of the EVs (N = 3) were measured by dynamic light scattering showing negative surface charge and moderate colloidal stability.

(E) Immunoblotting analysis showing the presence of characteristic EV markers TSG101, CD63, and CD81 in the isolated vesicles. β-actin served as the loading control. Blots are representative of three independent experiments.

(F and G) Nanoparticle tracking analysis (NTA) (N = 5) showing the concentration and size distribution of PLY(0.5) and naive EVs, respectively. The mean EV size is indicated showing smaller particle size in PLY-EVs compared to naive EVs.

(H) Quantification of relative total protein content of naive EVs and PLY(0.5)EVs by bicinchoninic acid protein assay (N = 3). $^{*}p < 0.05$ by unpaired t test.

(I) Relative efficacy of red blood cell lysis (N = 3) of PLYW433F toxoid mutant (0.5 μg/mL) as compared to wild-type PLY.

(J) NTA analysis (N = 5) showing the concentration of EVs purified from THP-1 cells challenged with 0.5 μg/mL of PLY-WT and PLY-W433F mutant. EVs purified from untreated cells served as control. $^{****}p < 0.0001$ by unpaired t test in (I and J). All data are represented as mean ± SEM. See also Figures S1, S2 and S13.

outward budding from the plasma membrane.[22] Susceptibility to PLY-induced cell death varies across cell types, with myeloid cells such as monocytes showing higher resistance as compared to lymphoid cells.[16] This is due to the preferential binding of PLY to the T cell membrane and the enhanced ability of monocytes to eliminate membrane pores through microvesicle shedding. However, the pathophysiological sequelae of EVs shed from intoxicated host cells are unknown. A recent study showed that PLY-induced microvesicles derived from HEK293 cells caused phenotypic changes in macrophages,[23] but this study was performed using synthetic PLY-bearing liposomes, which do not represent EVs shed from PLY-challenged immune cells. Since EVs transport cargo between cells,[24] it is intriguing to study the proteomic cargo of EVs shed from immune cells in response to PLY challenge and their implications on host response to infection. In this study, we investigated the fate and downstream consequences of PLY-induced EVs shed from challenged host cells.

Here, we found that the PLY-induced host EVs (PLY-EVs) are selectively enriched in innate immune and inflammatory proteins, which induce human monocyte-derived dendritic cell (DC) maturation and alert them to infection. *In vivo*, administration of PLY-EVs induced mortality and inflammation in zebrafish embryos. Using an intranasal challenge mouse model, we found that infection with wild-type pneumococci upregulated EV release in the lungs as compared to PLY-mutant strain. Adoptive transfer of EVs isolated from bronchoalveolar lavage of infected mice to healthy recipients induced pathology in a PLY-dependent manner. Our findings suggest that expelling PLY toxin pores through vesicles works as double-edged sword. While cells get rid of the damaged membrane with assembled toxin through vesicles to evade lysis, the released EVs harboring PLY and other inflammatory proteins induce cytotoxicity and inflammation within the host. Thus, host-EVs disseminate pore-forming toxin and other inflammatory cargo during infection that have dire consequences during infection.

RESULTS

Pneumolysin enhances shedding of extracellular vesicles from monocytes at sublytic doses

Myeloid cells, especially monocytes, show greater resistance to PLY-induced lysis in comparison to lymphoid cells, due to their enhanced vesicle shedding capacity.[16] Hence, we used human THP-1 monocytes as our model system to investigate the properties and fate of host vesicles shed in response to PLY. The conditioned culture supernatant was subjected to differential centrifugation to sequentially remove cell debris, apoptotic bodies, and larger microvesicles, followed by ultrafiltration to remove non-EV associated proteins. The EVs were subsequently precipitated using ExoQuick-TC reagent (System Biosciences) (Figure S1). THP-1 cells were stimulated with sublytic doses of recombinant His-tagged PLY (0.1, 0.5 μg/mL) for 24 h in culture medium pre-depleted of serum EVs, wherein the viability of the treated cells was found to be ~80% upon treatment (Figures S2A and S2B). A lytic dose of PLY (2 μg/mL) induced ~60% cell lysis and served as positive control. Inhibition of Ca^{2+}-dependent membrane repair processes using EDTA significantly reduced the cell viability by ~50% even at the sublytic PLY doses (Figure S2C). To capture the dynamics of PLY-induced EV shedding in real time, we performed high-speed confocal laser scanning microscopy of live THP-1 monocytes, which were labeled with the lipophilic membrane dye, Nile-red, and challenged with 0.5 μg/mL of PLY. By ~14 min post-stimulation, we found membrane budding and subsequent release of Nile-red positive vesicles from the plasma membrane (Figure 1A, Video S1). In contrast, untreated cells released relatively fewer EVs over the same time period (Figure 1A; Video S2). The morphology of the isolated EVs was visualized by negative contrast transmission electron microscopy (TEM), which showed that the particles were spheroid, membrane enclosed, and heterogeneous in size (Figure 1B). Size measurement indicated that the PLY-EVs were significantly smaller than Naive EVs (Figure 1C). Zeta potential measurements showed that the naive EVs and PLY(0.5)EVs were both negatively charged particles with moderate colloidal stability with values of −21.03 ± 3.27 mV and −16.6 ± 2.46 mV, respectively (Figure 1D).

Next, to confirm the identity of the isolated vesicles, we probed for the presence of characteristic EV markers by immunoblotting. The vesicles expressed the characteristic exosome markers—endosomal sorting complex required for transport (ESCRT-1) subunit, TSG101, and the tetraspanins CD63 and CD81 (Figure 1E). For measurement of particle size and quantification, we performed nanoparticle tracking analysis (NTA) and found that the PLY-EVs has relatively smaller particle size (mean 122.6 ± 4.4) compared to naive EVs (mean 204.1 ± 4.7 nm), showing the same trend as TEM analysis. More importantly, PLY(0.5)EVs had ~3-fold higher particle concentration as compared to naive EVs, suggesting upregulation of vesicle shedding upon PLY challenge (Figures 1F and 1G). In agreement with the NTA results, quantification of the total EV protein content by bicinchoninic acid (BCA) assay revealed PLY-EVs had ~2-fold higher protein abundance relative to naive EVs (Figure 1H). To investigate whether the pore-forming activity of PLY is essential for EV shedding from challenged cells, we quantified EVs shed

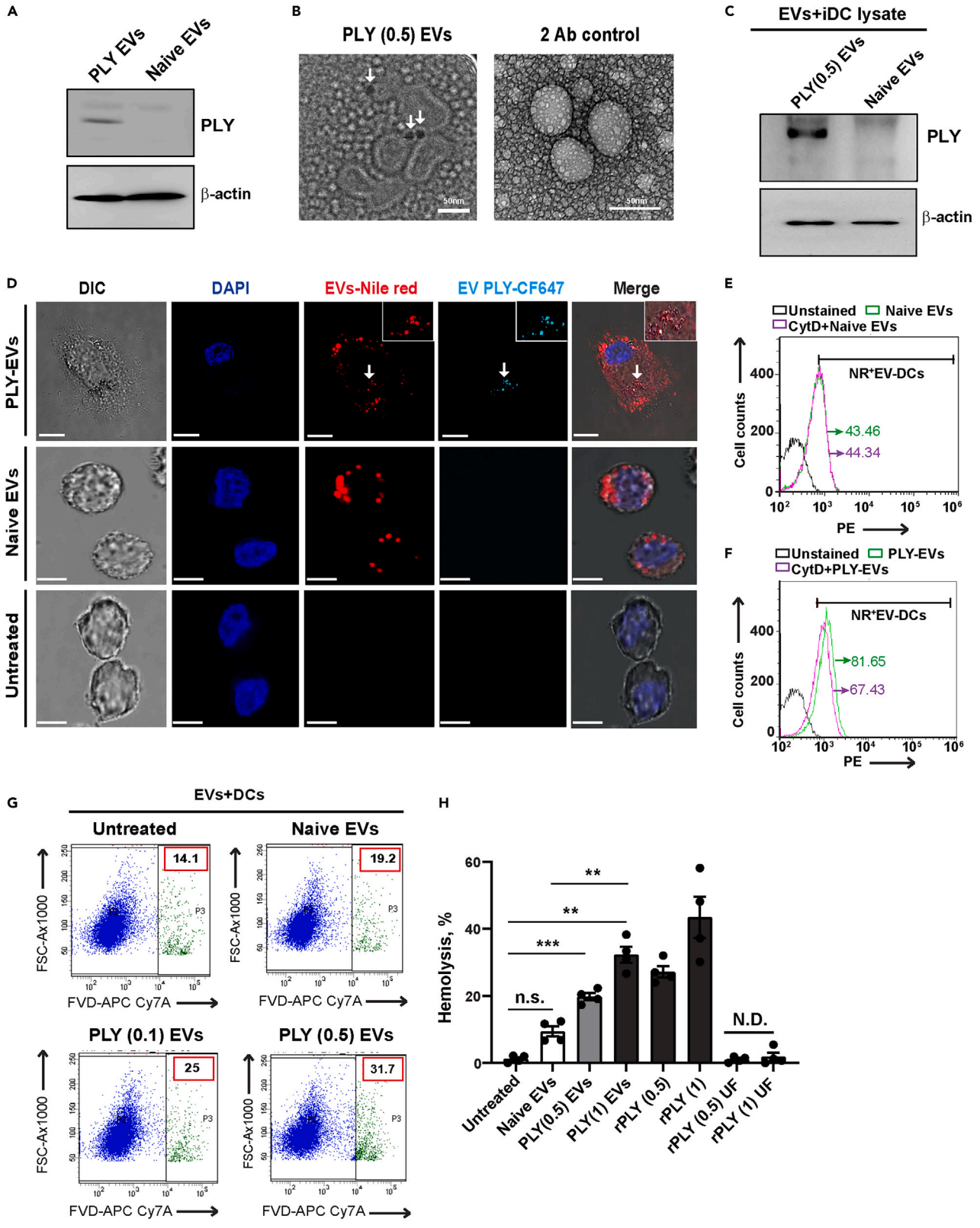
A
PLY EVs
Naive EVs
PLY
β-actin
B
PLY (0.5) EVs
2 Ab control
50nm
50nm
C
EVs+iDC lysate
PLY(0.5) EVs
Naive EVs
PLY
β-actin
D
DIC
DAPI
EVs-Nile red
EV PLY-CF647
Merge
PLY-EVs
Naive EVs
Untreated
E
Unstained
Naive EVs
CytD+Naive EVs
NR+EV-DCs
43.46
44.34
Cell counts
PE
F
Unstained
PLY-EVs
CytD+PLY-EVs
NR+EV-DCs
81.65
67.43
Cell counts
PE
G
EVs+DCs
Untreated
Naive EVs
PLY (0.1) EVs
PLY (0.5) EVs
14.1
19.2
25
31.7
P3
FSC-Ax1000
FVD-APC Cy7A
H
Hemolysis, %
n.s.
**
**
***
N.D.
Untreated
Naive EVs
PLY(0.5) EVs
PLY(1) EVs
rPLY (0.5)
rPLY (1)
rPLY (0.5) UF
rPLY (1) UF

Figure 2. Transfer of EV-bound PLY to recipient cells upon internalization induces hemolysis and cytotoxicity

(A) Immunoblots of EVs isolated from PLY (0.5 μg/mL) challenged and untreated THP-1 monocytes and probed using PLY monoclonal antibody. Blots are representative of two independent experiments.

(B) Transmission electron microscopy images ($N = 3$) showing immunogold labeling of PLY in EVs collected from THP-1 monocytes treated with 0.5 μg/mL of PLY. EVs stained with secondary antibody alone were used as control. Arrows point the gold bead (~12 nm) conjugated to secondary antibody. Scale bars, 50 nm.

(C) Immunoblotting of primary monocyte-derived immature DC lysates showing the transfer of PLY upon coincubation with PLY(0.5)EVs but not naive EVs for 24 h. β-actin served as the loading control. Blots are probed using anti-His antibody and representative of three independent experiments.

(D) Confocal microscopy of THP-1-monocyte-derived DCs incubated with PLY(0.5)EVs for 60 min showing the colocalization of EV-associated CF-647-labeled PLY (cyan) with the Nile-red-labeled EVs, on recipient DCs (magnified in inset). Scale bars, 10 μm.

(E and F) Flow cytometry analysis ($N = 2$) showing percentage of DCs with surface-bound Nile-red-labeled naive- (E) and PLY-EVs (F) upon coincubation for 60 min with or without pretreatment with 5 μm cytochalasin D (CytD).

(G) Viability staining of DCs ($N = 3$) treated with PLY EVs (0.1, 0.5) or naive EVs with fixable viability dye eFluor 780, showing the percentage of dead cells.

(H) Hemolysis assay ($N = 4$) showing the dose-dependent induction of red cell lysis upon addition of PLY EVs (0.5, 1) as compared to naive EVs. Recombinant PLY (rPLY) was used as positive control. rPLY-spiked medium passed through 100 kDa ultrafiltration spin columns (rPLY UF) was used as negative control to test for protein carry over into EV preparations. Data are represented as mean ± SEM. $^{**}p < 0.005$ and $^{***}p < 0.0005$ by one-way ANOVA with Tukey's multiple comparisons test. n.s., not significant. N.D., not detectable. See also Figures S3–S5 and S13.

by cells upon challenge with the attenuated PLY W433F toxoid mutant (PdB) that has diminished binding to membrane cholesterol and therefore significantly reduced hemolytic activity[25] (Figure 1I). By NTA analysis, we found that the toxoid mutant induced ~2-fold lower EVs as compared to wild-type PLY and equivalent to untreated cells (Figure 1J). The purified recombinant proteins, wild-type and toxoid PLY mutants, were tested for endotoxin and found to be < 10 ag/mL and 0.32 fg/mL, respectively, ruling out any effects due to LPS contamination (Figures S2D–S2G). Henceforth, individual EV preparations were used for each experiment after normalization of naive and PLY-EVs with respect to total protein content.

Transfer of EV-bound PLY to recipient cells upon internalization induces hemolysis and cytotoxicity

To investigate whether host cells expel membrane bound PLY into the shed EVs, we performed immunoblotting of EVs shed from PLY-challenged THP-1 monocytes using monoclonal PLY antibody. We detected PLY on the EVs shed from PLY-challenged cells but not on the naive EVs or untreated cells confirming the antibody specificity (Figure 2A). To examine the localization of PLY on the EVs, we performed immunogold labeling TEM analysis of PLY-EVs and found that PLY was localized on the EV membrane (Figures 2B and S3A–S3C). The percentage of the PLY-immunogold-labeled EVs was determined to be about ~30%, suggesting that cells shed both EVs containing and lacking PLY (Figure S3D). To visualize PLY release into EVs from challenged cells, we used recombinant GFP-tagged PLY protein having comparable activity as PLY-His protein (Figure S4A). Using high-speed confocal microscopy, we also demonstrated the dynamic release of GFP-tagged PLY from the membrane of challenged DiI-labeled monocytes through EVs (Videos S3 and S4). To verify that the released EVs contain PLY, we have measured line intensity profiles and quantified the Pearson and Mander's (M2) correlation coefficients confirming the colocalization of EVs (red) and GFP-PLY signals (Figures S4B and S4C). Besides, we also analyzed snapshots from the live-imaging video showing budding of EVs containing GFP-PLY and subsequent loss of GFP signal from the budding site, confirming that cells shed membrane-bound PLY through EVs (Figures S5A and S5B). The fate and downstream consequences of the shed-EV-associated PLY are unknown. We hypothesized that the EV-membrane localized PLY might be transferred onto the recipient cells upon EV internalization and cargo delivery. It has been proposed that vesicle uptake by target host cells could result in the insertion of the EV membrane on the target plasma membrane and delivery of EV cargo into the cytoplasm of recipient cells.[26] To test this hypothesis, we incubated primary human monocyte-derived immature dendritic cells (DCs) with purified PLY and naive EVs for 24 h, washed, and subsequently probed the cell lysates for PLY by immunoblotting. Results showed that cells coincubated with PLY-EVs, but not naive EVs, showed the presence of PLY protein, suggesting transfer of PLY from EVs to recipient cells upon vesicle internalization (Figure 2C). To quantify PLY content in the EVs, we performed densitometry analysis using recombinant PLY as standard and found it to be 6.8 ng/μg of total EV protein (Figures S5C and S5D). Strikingly, EVs purified from cells challenged with wild-type PLY had ~3-fold higher PLY content relative to EVs isolated from PLYW433F-toxoid-challenged cells (Figure S5E). To unequivocally demonstrate the transfer of EV-associated PLY to recipient cells, we purified EVs from monocytes challenged with CF647-labeled PLY and labeled the EVs with Nile-red. The labeled EVs were subsequently incubated with THP-1-monocyte-derived DCs for 1 h. Clearly, colocalization of Nile-red signal (EVs) and CF647-PLY confirmed the specific transfer of EV-bound PLY to recipient cells upon internalization (Figure 2D). To test whether the EV internalization by target cells is independent of actin-mediated endocytosis, THP-1-monocyte-derived DCs were pretreated with the actin polymerization inhibitor, cytochalasin D, for 30 min prior to incubation with Nile-red-labeled EVs, and subsequently the binding of EVs was assessed by flow cytometry. We found that there was only a slight reduction in percentage of Nile-red EV-positive DCs upon cytochalasin D pretreatment, indicating that EV uptake occurs independently of actin-dependent endocytosis (Figures 2E and 2F). Consistent with the transfer of EV-associated PLY to recipient DCs, we found that PLY-EVs induced higher cytotoxicity in a dose-dependent manner in recipient DCs as compared to naive EVs (Figure 2G). In order to test whether the PLY-EVs are hemolytic, we incubated normalized protein equivalents of PLY-EVs and naive EVs with whole blood collected from healthy donors. Results showed that PLY-EVs, but not naive EVs, induced hemolysis in a dose-dependent manner (Figure 2H). Recombinant PLY (rPLY) was used as a positive control. To rule out carryover of non-EV-bound PLY from culture supernatant into the EV preparations, rPLY-spiked medium was passed through the 100 kDa ultrafiltration columns akin to EV isolation. The retentate fraction was checked for PLY-hemolytic activity and found to be negative. This confirmed that the measured hemolysis

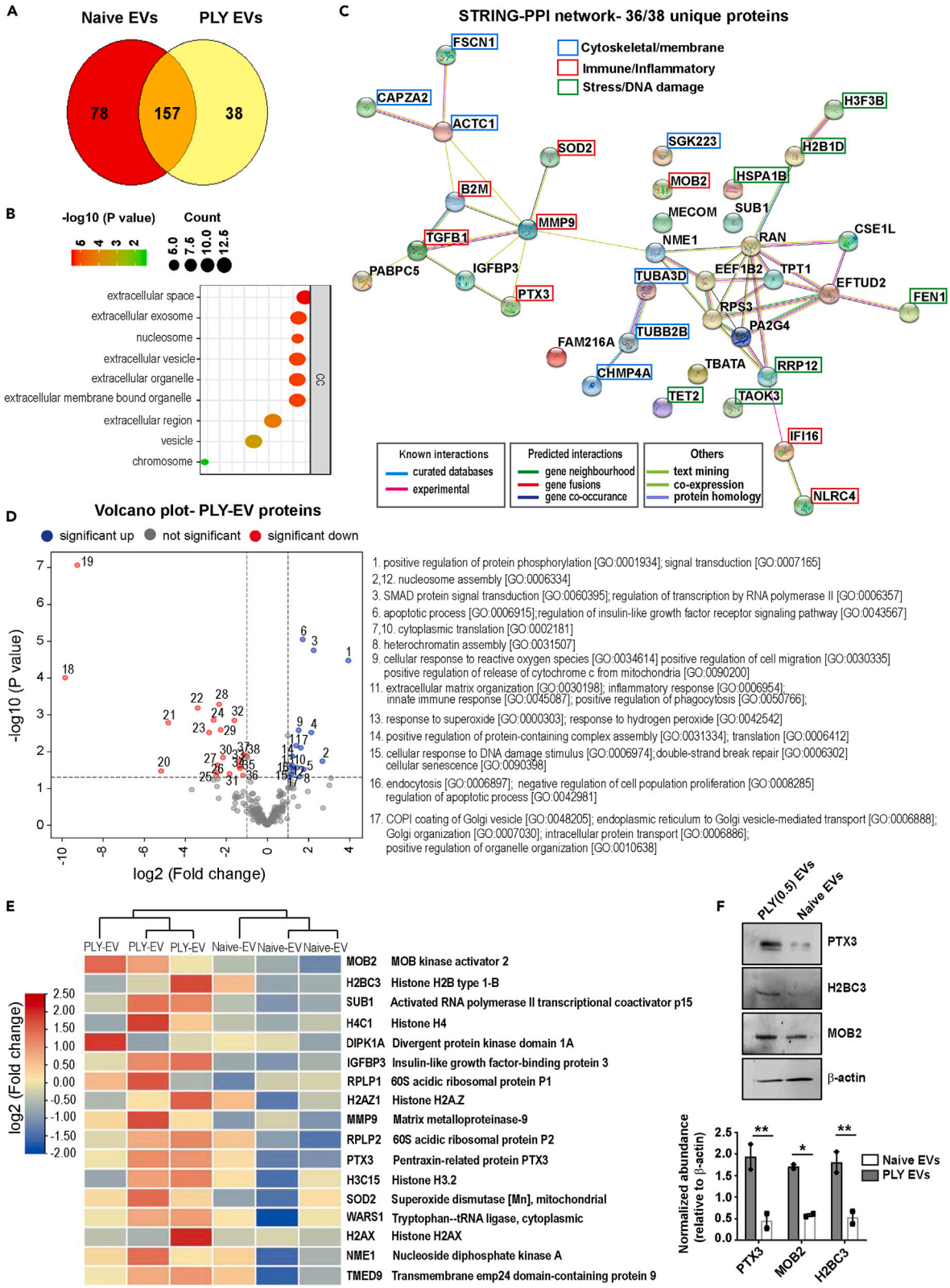
A
Naive EVs
PLY EVs
78
157
38
B
-log10 (P value)
Count
6
4
3
2
6.0
7.5
10.0
12.5
extracellular space
extracellular exosome
nucleosome
extracellular vesicle
extracellular organelle
extracellular membrane bound organelle
extracellular region
vesicle
chromosome
CC
C
STRING-PPI network- 36/38 unique proteins
Cytoskeletal/membrane
Immune/Inflammatory
Stress/DNA damage
FSCN1
CAPZA2
ACTC1
SOD2
B2M
MMP9
TGFB1
PABPC5
IGFBP3
PTX3
SGK223
MOB2
MECOM
NME1
TUBA3D
TUBB2B
FAM216A
CHMP4A
TBATA
TET2
TAOK3
IFI16
NLRC4
H3F3B
H2B1D
HSPA1B
SUB1
RAN
CSE1L
EEF1B2
TPT1
EFTUD2
FEN1
RPS3
PA2G4
RRP12
Known interactions
curated databases
experimental
Predicted interactions
gene neighbourhood
gene fusions
gene co-occurance
Others
text mining
co-expression
protein homology
D
Volcano plot- PLY-EV proteins
significant up
not significant
significant down
-log10 (P value)
log2 (Fold change)
1. positive regulation of protein phosphorylation [GO:0001934]; signal transduction [GO:0007165]
2,12. nucleosome assembly [GO:0006334]
3. SMAD protein signal transduction [GO:0060395]; regulation of transcription by RNA polymerase II [GO:0006357]
6. apoptotic process [GO:0006915]; regulation of insulin-like growth factor receptor signaling pathway [GO:0043567]
7,10. cytoplasmic translation [GO:0002181]
8. heterochromatin assembly [GO:0031507]
9. cellular response to reactive oxygen species [GO:0034614] positive regulation of cell migration [GO:0030335] positive regulation of release of cytochrome c from mitochondria [GO:0090200]
11. extracellular matrix organization [GO:0030198]; inflammatory response [GO:0006954]; innate immune response [GO:0045087]; positive regulation of phagocytosis [GO:0050766];
13. response to superoxide [GO:0000303]; response to hydrogen peroxide [GO:0042542]
14. positive regulation of protein-containing complex assembly [GO:0031334]; translation [GO:0006412]
15. cellular response to DNA damage stimulus [GO:0006974]; double-strand break repair [GO:0006302] cellular senescence [GO:0090398]
16. endocytosis [GO:0006897]; negative regulation of cell population proliferation [GO:0008285] regulation of apoptotic process [GO:0042981]
17. COPI coating of Golgi vesicle [GO:0048205]; endoplasmic reticulum to Golgi vesicle-mediated transport [GO:0006888]; Golgi organization [GO:0007030]; intracellular protein transport [GO:0006886]; positive regulation of organelle organization [GO:0010638]
E
PLY-EV
PLY-EV
PLY-EV
Naive-EV
Naive-EV
Naive-EV
log2 (Fold change)
MOB2 MOB kinase activator 2
H2BC3 Histone H2B type 1-B
SUB1 Activated RNA polymerase II transcriptional coactivator p15
H4C1 Histone H4
DIPK1A Divergent protein kinase domain 1A
IGFBP3 Insulin-like growth factor-binding protein 3
RPLP1 60S acidic ribosomal protein P1
H2AZ1 Histone H2A.Z
MMP9 Matrix metalloproteinase-9
RPLP2 60S acidic ribosomal protein P2
PTX3 Pentraxin-related protein PTX3
H3C15 Histone H3.2
SOD2 Superoxide dismutase [Mn], mitochondrial
WARS1 Tryptophan--tRNA ligase, cytoplasmic
H2AX Histone H2AX
NME1 Nucleoside diphosphate kinase A
TMED9 Transmembrane emp24 domain-containing protein 9
F
PLY(0.5) EVs
Naive EVs
PTX3
H2BC3
MOB2
β-actin
Normalized abundance (relative to β-actin)
Naive EVs
PLY EVs
PTX3
MOB2
H2BC3

Figure 3. PLY-EVs are enriched for proteins involved in immune response and inflammation

(A) Venn-diagram plot of proteins identified in naive and PLY-EVs by LC-MS/MS analysis.

(B) Cellular component gene ontology analysis for exosome proteins that were enriched in PLY-EVs, using G-profiler using p value cutoff score of $p < 0.05$.

(C) STRING protein interaction network analysis of proteins unique to PLY-EVs. A total of 54 interactions (edges) linking 36 proteins (nodes) were observed. The average local clustering coefficient was 0.514 and protein-protein interaction enrichment p value was 3.12E-08, which demonstrated significant interactions among proteins.

(D) Volcano plot analysis of differential protein abundance in PLY(0.5)EVs as compared to naive-EVs. Blue and red shows differentially enriched and depleted proteins, respectively, with fold change > ± 2 and $p < 0.05$. The biological process gene ontology analysis for the exosomal proteins enriched in PLY-EVs is shown.

(E) Heatmap showing the log fold enrichment of significantly enriched proteins in PLY(0.5)EVs compared to naive EVs with log fold change of ± 2. Proteomics data are representative of three biological replicates.

(F) Western blotting and densitometry analysis showing the enrichment of three inflammatory proteins, Ptx3, histone H2BC3, and MOB2, in PLY-EVs, relative to naive EVs as identified by LC-MS/MS. Blots are representative of two independent experiments. Data are represented as mean ± SEM. *$p < 0.05$ and **$p < 0.01$ by two-way ANOVA with Bonferroni's multiple comparisons test. See also Figure S13.

was solely mediated by the EV-associated PLY. Together, our results suggest that PLY-EVs transfer PLY pores to recipient cells upon EV internalization, thereby mediating cytolysis.

PLY-EVs are enriched for proteins involved in immune response and inflammation

To study the differential protein cargo of the PLY-EVs relative to naive EVs, we performed mass spectrometry analysis of the EV lysates upon normalization of samples with respect to total protein content. We identified 157 host proteins common to both naive and PLY EVs and 38 unique proteins in PLY-EVs (Figure 3A). Cellular component (CC) gene ontology analysis revealed that the PLY-EVs were significantly enriched for proteins associated with exosomes, extracellular vesicles, and nucleosome (Figure 3B). The STRING PPI protein-interaction network analysis revealed that the unique interactome of PLY-EVs consisted of 54 interactions (edges) linking 36 proteins (nodes) (Figure 3C). The average local clustering coefficient was 0.514, and the protein-protein interaction enrichment p value was 3.12E-08, which demonstrated significant interactions among EV cargo proteins. We found cytoskeletal proteins, actin and tubulin; RhoA activator, SGK223; membrane ruffling protein, FSCN1; and ESCRT-III protein, CHMP4A that are involved in exosome biogenesis and release through membrane projections. Besides, we found many other proteins involved in cellular stress responses such as heat shock protein, HSPA1B, DNA damage and repair proteins, endonuclease FEN1, p53 regulator, RRP12, and the p38/MAPK14-stress-activated MAPK cascade regulator, TAOK3. The presence of DNA repair proteins in PLY-EVs is in agreement with a previous study by Rai et al., 2016,[27] showing that PLY induces DNA double-strand breaks in host cells. Notably, we found several proteins involved in immune defense and inflammatory signaling exclusively in PLY-EVs, such as the gamma-interferon-inducible protein, IFI16; MHC-I component B2M; NLR family CARD domain containing protein 4 (NLRC4); complement activating long pentraxin, PTX3; matrix metalloproteinase, MMP9; and superoxide dismutase, SOD2 (Figure 3C).

Differential protein content of PLY-EVs relative to naive EVs was classified based on the cutoff for fold change > ± 2 and $p < 0.05$ to create the volcano plot (Figure 3D). Gene ontology analysis of the enriched proteins in PLY-EVs revealed that they influence major biological processes like endocytosis, vesicle trafficking, apoptosis, cellular response to reactive oxygen species, cellular senescence, extracellular matrix organization, and innate immune and inflammatory responses. Heatmap analysis of the significantly enriched proteins identified the serine threonine kinases activator, MOB2, that regulates DNA damage response[28] and cell-cycle progression[29] in cancer cells (Figure 3E). MOB2 has been shown to activate the downstream kinases, NDR1/2, that play pivotal role in inflammatory cytokine signaling and antimicrobial innate immune response.[30] Besides, we identified canonical and histone variants such as H2B, H4, H3.2, H2A.Z, and H2AX to be significantly enriched in PLY-EVs as compared to naive EVs. Histones have been reported to be enriched in exosomes,[31] consistent with the theory that cells get rid of damaged DNA by packaging them into exosomes to prevent type I interferon (IFN) release via the c-GAS STING pathway.[32] Besides their well-established roles in nuclear chromatin organization, cationic histones have been proposed to have antimicrobial activity by disrupting bacterial membrane.[33] Key inflammatory proteins PTX3, MOB2, and H2BC3 shown to be enriched in PLY-EVs by proteomics were validated by western blotting (Figure 3F). Hence, the consequence of histones that are enriched in the PLY-EVs on the bacterial fitness during an infection remains to be investigated. Taken together, our results identified that PLY-EVs contain antimicrobial stress response and inflammatory proteins that could modulate the host response to infection.

PLY-EVs induce dendritic cell maturation and inflammatory cytokine release upon internalization

To investigate the effects of PLY-EVs on immune cells, we tested their internalization by DCs, which are the major antigen-presenting cells and the resulting consequences on DC activation. We incubated CFSE-labeled EVs with THP-1-monocyte-derived DCs (Figure S6) for 24 h and visualized their internalization by confocal microscopy. Results showed that PLY-EVs were internalized to a greater extent by the DCs than naive EVs (Figure 4A). The EV uptake was also quantified by flow cytometry, confirming the higher uptake of PLY-EVs relative to naive EVs in a dose-dependent manner (Figures 4B, 4C, and S7A–S7D). Interestingly, we also found that PLY-EVs, but not naive EVs, induced dendritic processes that are characteristic of maturation in stimulated day 5 immature THP-1-monocyte-derived DCs (iDCs) upon coincubation for 24 h (Figure 4D). To verify the DC maturation induced by PLY-EVs, we quantified the expression of typical DC activation markers by flow cytometry. Consistent with Figure 4D, we found that iDCs incubated with PLY-EVs, but not naive EVs, upregulated the surface expression of costimulatory molecules, CD80 and CD86, as well as the maturation marker, CD83 (Figures 4E–4G and S7E–S7J). The maturation of THP-1-monocyte-derived DCs by PLY-EVs was verified in primary monocytes isolated from healthy donors upon coincubation with naive and PLY-EVs for

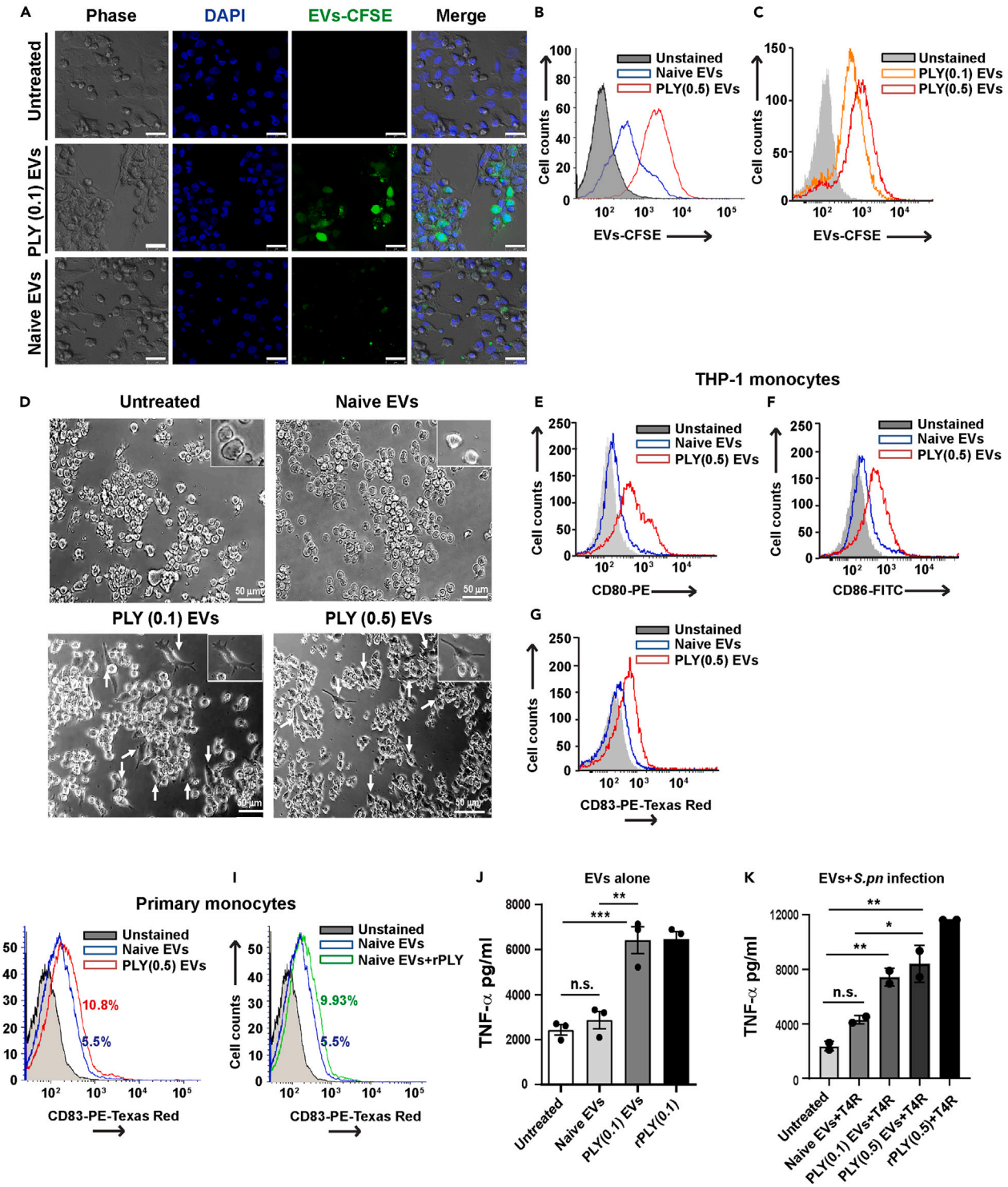

Figure 4. PLY-EVs induce dendritic cell maturation and inflammatory cytokine release upon internalization

(A) Confocal microscopy images showing the internalization of CFSE-labelled PLY (0.1) and naive EVs (green) by THP-1-monocyte-derived DCs at 24 h post-treatment. Scale bars, 25 μm.

(B) Flow cytometry histograms (N = 3) to quantify the DC uptake of CFSE-labeled PLY(0.5)EVs and naive EVs.

(C) Dose-dependent uptake of PLY (0.1, 0.5) EVs by DCs.

Figure 4. *Continued*

(D) Phase-contrast microscopy images of immature day 5 DCs coincubated with PLY (0.1, 0.5) EVs and naive EVs for 24 h. Arrows indicate matured DCs (magnified in inset). Scale bars, 50 μm. Images are representative of three independent experiments.

(E–G) Flow cytometry histograms ($N = 3$) to quantify the expression levels of (E) CD80, (F) CD86, and (G) CD83 on THP-1-monocyte-derived DCs treated with PLY(0.5) and naive EVs.

(H and I) Flow cytometry histograms ($N = 2$) showing the expression levels of DC maturation marker CD83 at 96 h post-incubation of primary human monocytes with (H) PLY(0.5) and naive EVs and (I) naive EVs pre-treated with recombinant PLY protein (naive EVs+rPLY).

(J and K) Cytokine ELISA showing the levels of secreted TNF-α from (J) DCs treated with PLY (0.1) EVs or naive EVs alone ($N = 3$) for 24 h and (K) DCs pre-treated with PLY (0.1,0.5) or naive EVs for 24 h followed by subsequent infection with *S. pneumoniae*, T4R strain ($N = 2$). Recombinant PLY (0.5 μg/mL) was used as positive control. All data are represented as mean ± SEM. $^{*}p < 0.05$, $^{**}p < 0.005$, and $^{***}p < 0.001$ by one-way ANOVA with Tukey's multiple comparisons test. n.s., not significant. See also Figures S6–S9.

96 h. The PLY-EV-treated primary monocytes showed CD83 upregulation (Figures 4H and S8A–S8D) and differentiation into characteristic dendritic cell morphology as compared to naive EV-treated cells (Figures S8E and S8F). As control, naive-EVs that were pretreated with recombinant purified PLY protein for 30 min and subsequently incubated with primary monocytes also induced differentiation into DC phenotype and CD83 upregulation (Figures 4I and S8A–S8F).

Similar to PLY-EVs, EVs isolated from THP-1 monocytes infected with *S. pneumoniae* serotype 4 strain, T4R (T4R-EVs), showed higher internalization by A549 human alveolar basal epithelial cells as compared to EVs obtained from cells infected with isogenic PLY mutant strain, T4RΔply (T4RΔply-EVs) (Figures S9A and S9B). Next, we tested the consequence of EV internalization by THP-1-monocyte-derived DCs on the cellular inflammatory cytokine response. We found that PLY-EV-treated DCs released higher levels of the inflammatory Th1-polarizing cytokines, tumor necrosis factor alpha (TNF-α) (Figure 4J), and interleukin-12 (IL-12) (Figure S9C), as compared to cells treated with naive EVs. Based on our findings suggesting the immunostimulatory potential of PLY-EVs, we hypothesized that EVs shed from PLY-challenged cells could prime bystander naive cells to stronger response upon infection. To test this, DCs were pretreated with PLY-EVs or naive EVs for 24 h and subsequently infected with *S. pneumoniae*, T4R strain, following which the secretion of the pro-inflammatory cytokine, TNF-α, was measured. Results showed that DCs pretreated with PLY-EVs produced significantly higher amounts of TNF-α upon infection (Figure 4K), when compared to naive-EV treated cells. In agreement, we found that EVs derived from monocytes infected with T4R strain induced higher TNF-α from DCs as compared to EVs from T4RΔply-infected cells (Figure S9D). Taken together, our findings show that PLY-EVs activate DCs upon internalization and boosts pro-inflammatory response during infection.

Administration of PLY-EVs induces inflammation and toxicity *in vivo*

To study the toxicity and pathophysiological effects of the toxin-induced host EVs *in vivo*, we first employed a zebrafish (*Danio rerio*) model, in which CFSE-labeled naive and PLY(0.5)EVs were microinjected into the duct of Cuvier of day 3 post-fertilization embryos. Zebrafish is a widely accepted model system for human infectious diseases due to their optical transparency and similarity with the human immune system[34] and have been previously validated by us[35] and others[36] as a suitable model to study pneumococcal pathogenesis. We found that zebrafish administered with labeled PLY-EVs, but not naive EVs, developed severe pericardial edema at day 2 post-injection, confirming the toxicity of PLY-containing EVs (Figure 5A). Embryo E3-medium-treated embryos served as the mock-injected group. The PLY-EV-administered group also showed a progressive decline in the heartbeat rate as compared to naive EV and mock-injected control groups, indicative of cardiac dysfunction (Figure 5B). In conjunction with the severe cardiac dysfunction and edema formation, the PLY-EV-treated zebrafish also showed a significantly lower survival rate compared to naive EV and mock-injected group, with only 30% of the embryos surviving at day 4 post-injection (Figure 5C). Moreover, zebrafish administered with PLY-EVs showed ~2.5-log-fold higher expression of the pro-inflammatory cytokine TNF-α relative to naive-EV-treated group (Figure 5D).

Next, we used a mouse toxin challenge model to investigate the toxicity of PLY-induced EVs. To mimic PLY-induced acute lung injury during infection, 6- to 8-week-old C57BL/6 mice were intranasally administered with purified recombinant PLY toxin. The PLY dose was chosen based on previous studies showing the pathophysiologically relevant dose that induces acute lung injury,[37] transmission of pneumococci,[38] and restoration of virulence in non-hemolytic strains.[39] We tested two intranasal doses of 0.25 and 0.5 μg PLY, but mortality was observed at 0.5 μg dose. Hence, we adopted an intranasal dose of 0.25 μg PLY in 50 μL PBS (5 μg/mL) to model PLY-induced acute lung injury. We found that by 18 h after PLY administration, mice showed a significant increase in lung vascular permeability, as visualized by extravasation of the intravenously administered plasma tracer dye, Evans blue, through IVIS imaging (Figure S10A). This was concomitant with the presence of GFP-tagged PLY in the lungs of treated mice (Figure S10B). PLY-induced lung inflammation was also confirmed by higher infiltration of neutrophils and macrophages into the lungs (Figure S10C). Histological staining revealed regions of tissue microlesions and immune cell infiltration into the alveolar spaces of the PLY-treated mice (Figure S10D). At 18 h, EVs were isolated from murine bronchoalveolar lavage fluid (BALF), collected by lung perfusion postmortem. The EVs isolated from untreated and PLY-treated donor mice were subsequently administered intranasally to healthy recipient mice (18 μg/mouse). At 18 h after EV administration, the bioavailability of the Nile-red-labeled EVs in the murine respiratory tract was visualized by IVIS imaging. Results showed that the PLY-EVs showed higher accumulation even at 18 h as compared to naive-EVs derived from untreated mice (Figure 5E). PBS-administered mice served as negative control. Strikingly, we found that mice challenged with wild-type PLY produced ~2-fold higher amount of EVs (Figure S10E) and harbored higher PLY content as compared to the PLYW433F toxoid mutant (Figure S10F). These results are in agreement with data from *in vitro* experiments (Figures 1J and S5E). Flow cytometry analysis of the murine BALF revealed an upregulation of neutrophils (Figures 5F and S11) and macrophages (Figures 5G and S11) in

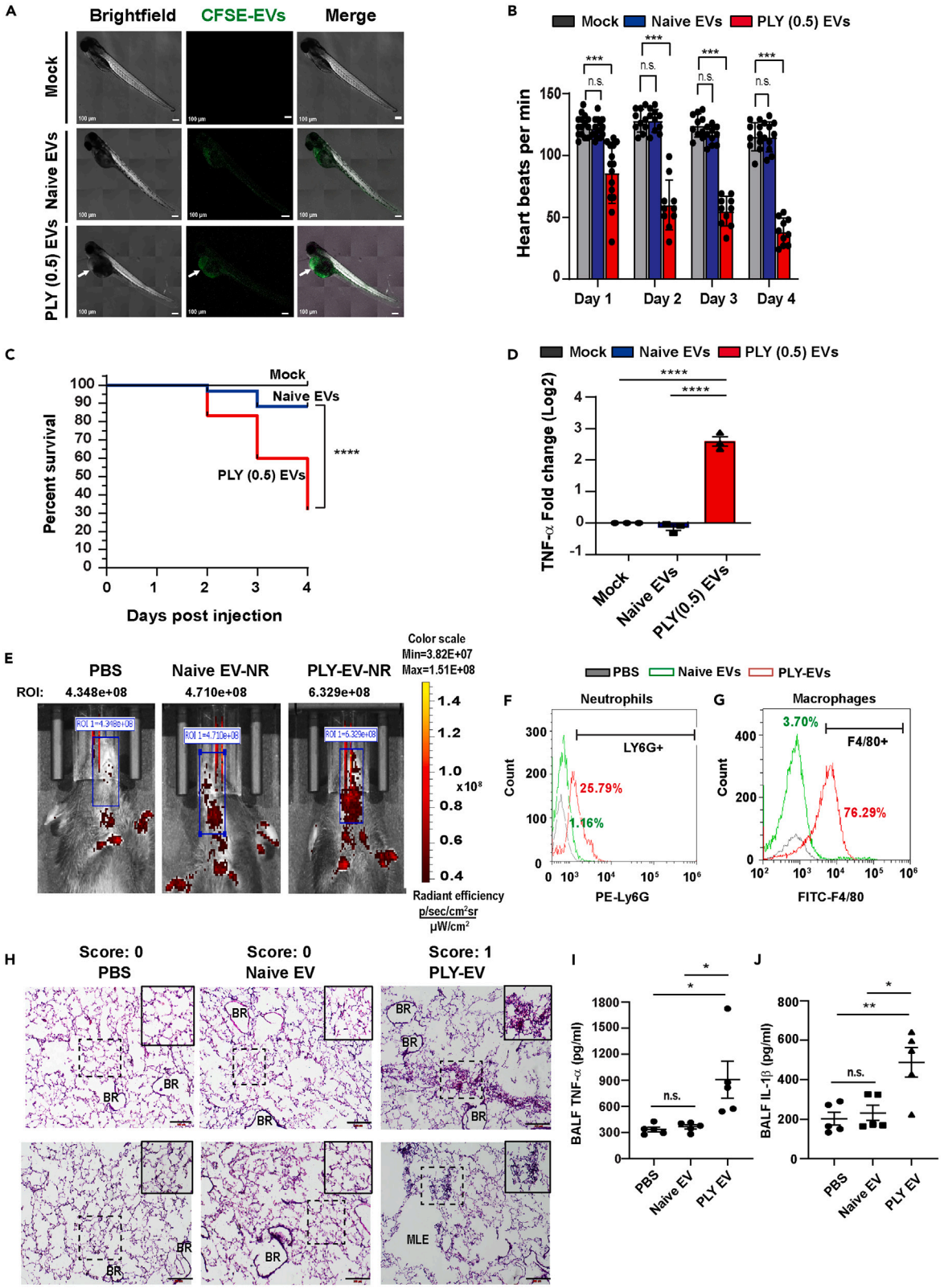
A
Brightfield
CFSE-EVs
Merge
Mock
Naive EVs
PLY (0.5) EVs
B
Mock
Naive EVs
PLY (0.5) EVs
Heart beats per min
Day 1
Day 2
Day 3
Day 4
C
Mock
Naive EVs
PLY (0.5) EVs
Percent survival
Days post injection
D
Mock
Naive EVs
PLY (0.5) EVs
TNF-α Fold change (Log2)
E
PBS
Naive EV-NR
PLY-EV-NR
ROI:
4.348e+08
4.710e+08
6.329e+08
Color scale
Min=3.82E+07
Max=1.51E+08
Radiant efficiency
p/sec/cm²sr
μW/cm²
F
PBS
Naive EVs
PLY-EVs
Neutrophils
LY6G+
25.79%
1.16%
PE-Ly6G
G
Macrophages
3.70%
F4/80+
76.29%
FITC-F4/80
H
Score: 0
PBS
Score: 0
Naive EV
Score: 1
PLY-EV
BR
MLE
I
BALF TNF-α (pg/ml)
PBS
Naive EV
PLY EV
J
BALF IL-1β (pg/ml)
PBS
Naive EV
PLY EV

Figure 5. Administration of PLY-EVs induces inflammation and toxicity *in vivo*

(A) Confocal microscopy of zebrafish embryos (N = 60 embryos) injected with CFSE-labeled naive or PLY(0.5)EVs (green) at day 2 post-injection showing the development of pericardial edema in the PLY-EV-treated group (arrows). Scale bars, 100 μm.

(B and C) Heartbeat (N = 15/group) and (C) survival of zebrafish (N = 60 embryos) injected with naive or PLY(0.5)EVs was monitored up to 4 days post-injection. *** in (B) denotes $p < 0.001$ by Mann-Whitney (two-tailed) test. **** in (C) denotes $p < 0.0001$ by Log rank (Mantel-Cox) test. n.s., not significant.

(D) Real-time PCR experiment (N = 3) showing the relative expression of TNF-α in zebrafish treated with naive or PLY(0.5)EVs at day 4 relative to mock-injected group. ****$p < 0.0001$ by one-way ANOVA with Tukey's multiple comparisons test. Data in (B and D) represent mean ± SD.

(E) IVIS imaging of C57BL/6 mice administered intranasally with Nile-red-labeled EVs (18 μg/mice) purified from BALF of PBS- (naive EVs) or PLY-challenged mice (PLY-EVs). ROI intensity values indicate the total flux (photons/sec) recorded from the given region showing higher intensity of PLY-EVs in the respiratory tract. The color scale (photons/sec/cm^2) indicates the relative intensities of individual signals.

(F and G) Flow cytometry analysis of neutrophils (Ly6G$^+$) and inflammatory macrophages (F4/80$^+$) in BALF of mice (N = 6 mice/group) administered with naive EVs or PLY-EVs at 18 h post-treatment.

(H) Hematoxylin and eosin (H&E) staining of mouse lungs (N = 6 mice/group) at 18 h post-treatment with PLY-EVs, naive EVs, or PBS. Mice treated with PLY-EVs showed tissue microlesions (MLE) and immune infiltration in the alveolar interstitium indicative of PLY-induced tissue damage (magnified in the inset). BR, bronchiole; MLE, microlesions. Scale bars, 200 μm. Blind histopathological scoring was performed based on presence or absence of cellularity in alveolar interstitium and lesions. A score of "0" was given when no lesions were found, and score of "1" was given to tissue showing increasing cellularity and lesions.

(I and J) Levels of pro-inflammatory cytokines (I) TNF-α and (J) IL-1β in the murine BALF (N = 5 mice/group) upon treatment with naive EVs or PLY-EVs were measured post-sacrifice at 18 h. PBS-treated mice served as negative control. Mouse BALF flow cytometry and histology data are representative of three independent experiments. Data are represented as mean ± SEM. * in (I and J) indicates $p < 0.05$ and **$p < 0.01$ by one-way ANOVA with Tukey's multiple comparisons test. n.s., not significant. See also Figures S10 and S11.

lungs of mice treated with PLY-EVs, in comparison to naive-EV- and PBS-treated groups. This was also confirmed by lung histology that showed microlesions and inflammatory cell infiltration into the alveolar interstitium of PLY-EV-treated mice (Figure 5H). Naive-EV- and PBS-treated mice had normal lung morphology with intact alveolar space and absence of inflammatory cells. Further, PLY-EV-treated mice showed significantly higher levels of the pro-inflammatory cytokines, TNF-α (Figure 5I) and IL-1β (Figure 5J), in the BALF at 18 h when compared to naive-EV- and PBS-treated mice. Taken together, our results show that the PLY-EVs induce toxicity and inflammation *in vivo*.

Adoptive transfer of EVs from infected mice drives inflammation and pathology in a PLY-dependent manner

To verify the significance of host-derived EVs shed during pneumococcal infection, we intranasally challenged C57BL/6 mice with 4 × 10^6 CFU of serotype 4 encapsulated strain, T4 or the PLY mutant strain, T4Δply. The mice were monitored daily for clinical symptoms and sacrificed at 4 days post-infection. EVs were isolated from the BALF of infected mice postmortem (Figure 6A). Mice infected with the wild-type T4 strain had significantly higher bacterial load in the BALF as compared to the T4Δply-infected mice (Figure 6B). Importantly, EV quantification using a total protein analysis revealed ~2-fold higher EV abundance in BALF of T4-infected mice as compared to mice infected with T4Δply strain (Figure 6C). The EVs purified from infected mice were normalized according to protein content, labeled with Nile-red and administered intranasally to healthy recipient mice (35 μg/mouse) to study their effects. At 18 h post-EV transfer, IVIS imaging revealed that EVs from T4-infected mice showed higher retention in respiratory tract of recipient mice, when compared to EVs from T4Δply-infected or uninfected mice (Figure 6D). Flow cytometry analysis revealed higher abundance of inflammatory macrophages (Figures 6E, S12A, and S12C) and neutrophils (Figures 6F, S12B, and S12D) in the BALF of mice treated with EVs isolated from T4-infected mice, relative to T4Δply infected. In agreement, we also found higher levels of the pro-inflammatory cytokine TNF-α in the BALF of recipient mice upon treatment with T4-EV, relative to T4Δply-EVs and naive EVs (Figure 6G). Correlating with higher TNF-α release and immune cell infiltration induced by EVs from T4-infected mice, lung histology revealed tissue damage as observed by the microlesions as well as the presence of infiltrated cells within the alveolar interstitium (Figure 6H). Mice treated with EVs from uninfected mice showed normal lung morphology, whereas EVs from T4Δply mice showed substantially lesser tissue damage compared to EVs from T4 infection. Overall, our data provides compelling evidence to suggest that EVs shed by host cells during pneumococcal infection drives inflammation and tissue damage in a PLY-dependent manner.

DISCUSSION

Pneumolysin (PLY), the β-barrel pore-forming toxin released by the respiratory tract pathogen *S. pneumoniae* binds to membrane cholesterol of eukaryotic host cells and oligomerizes to form transmembrane pores, resulting in lytic cell death.[12] In this study, we found that stimulation of human THP-1 monocytes with sublytic doses of recombinant PLY upregulates extracellular vesicle shedding. Further, we also showed that the shed EVs harbor membrane-localized PLY, which is in agreement with previous studies that showed the expulsion of PLY pores from cells through microvesicle shedding.[14,16,40] However, the downstream effects of the shed PLY-EVs on the host response during infection are unknown, and it was reported that the pore-forming toxins are completely neutralized upon capture by synthetic-cholesterol-containing liposomes.[41–43] However, neither of these studies investigated the downstream effects of the toxin-soaked liposomes. Moreover, synthetic liposomes differ from host-cell-derived EVs with regard to membrane lipid composition, as well as the absence of surface proteins that mediate cell tropism and fusion with target cells.[44] Our findings reveal that EVs shed from PLY-intoxicated host cells harbor membrane-bound PLY and induces dose-dependent hemolysis and cytotoxicity in recipient cells upon internalization. This was confirmed by experiments showing the incorporation of labeled EV-membrane associated PLY into recipient monocyte-derived DCs upon coincubation. Our findings are in agreement with studies showing the transfer of EV-bound MHC-peptide complex to antigen-presenting cells upon membrane fusion, in a process

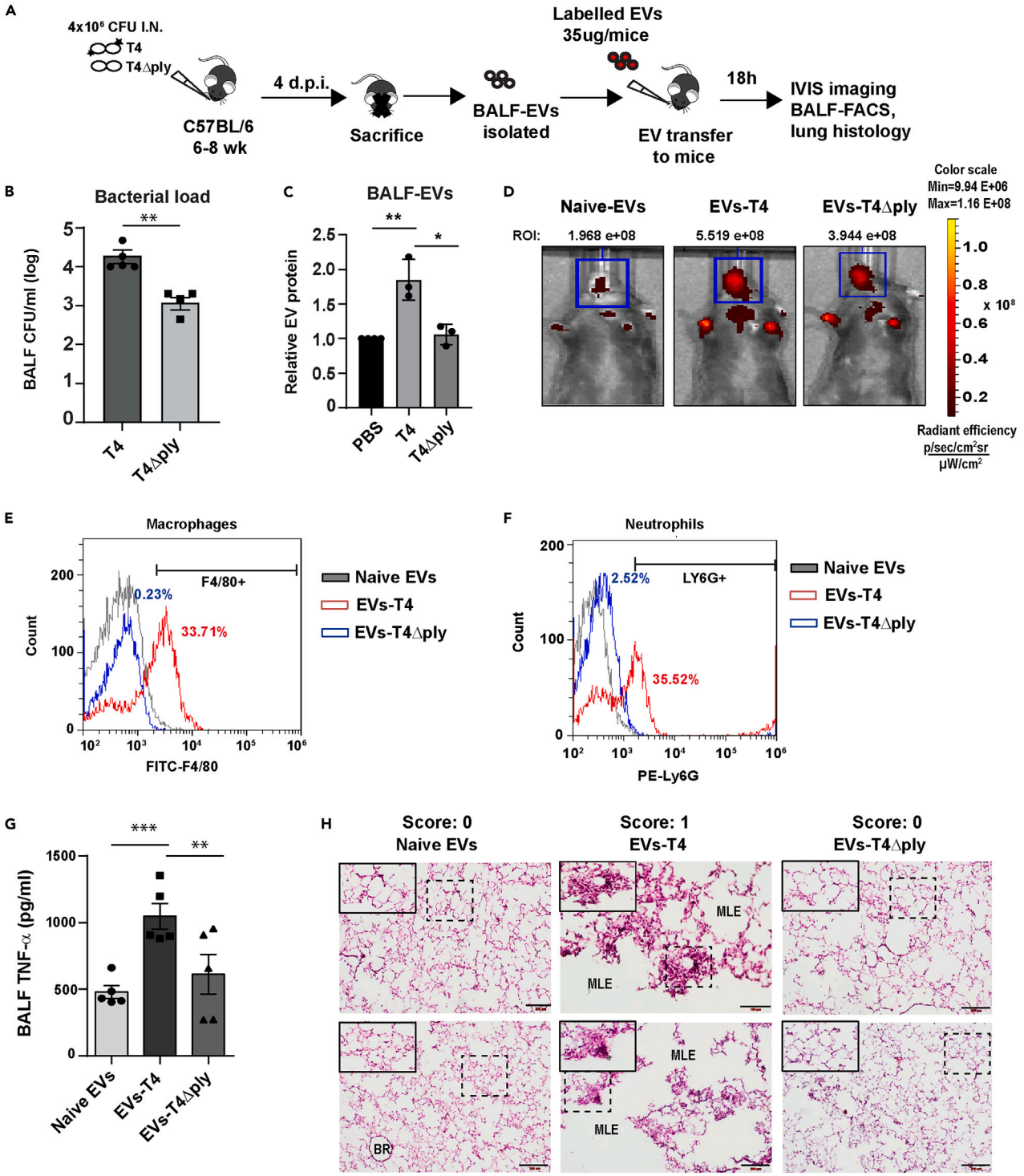

Figure 6. Adoptive transfer of EVs from infected mice drives inflammation and pathology in a PLY-dependent manner

(A) C57BL/6 mice were intranasally administered with 4 × 10^6 CFU of serotype 4 strain, T4 or the isogenic PLY mutant strain, T4Δply. At day 4 post-infection, EVs isolated from BALF were labeled and administered to healthy recipient mice at 35 μg/mice. The EV retention in murine respiratory tract was imaged by IVIS imaging and immune infiltration into lungs, and cytokine levels in BALF was measured.

(B) Bacterial load in murine BALF (N = 5 mice/group) upon infection with T4 and T4Δply strains was measured by CFU dilution assay. ** in (B) indicates $p < 0.01$ by Mann-Whitney test.

Figure 6. *Continued*

(C) Quantification of relative total EV protein content from mice ($N = 3$ mice/group) infected with T4 and T4Δply strains by BCA protein assay. PBS-treated mice served as control. * and ** in (C) indicates $p < 0.05$ and $p < 0.005$, respectively, by unpaired t test.

(D) IVIS imaging of mice intranasally administered with Nile-red-labeled EVs isolated from mice infected with T4 (EVs-T4) or T4Δply (EVs-T4Δply). EVs from PBS-treated mice (naive EVs) served as control. ROI intensity values indicate the total flux (photons/sec) recorded from the given region showing higher intensity of EVs from T4-infected mice in the respiratory tract. The color scale (photons/sec/cm^2) indicates the relative intensities of individual signals.

(E and F) Flow cytometry analysis of inflammatory macrophages (F4/80$^+$) and neutrophils (Ly6G$^+$) in BALF of mice ($N = 6$ mice/group) administered with EVs from infected or untreated mice at 18 h.

(G) TNF-α levels in the BALF of mice ($N = 5$ mice/group) treated with EVs isolated from infected or untreated mice were measured post-sacrifice at 18 h by ELISA. ** and *** in (G) indicates $p < 0.01$ and $p < 0.001$, respectively, by unpaired t test.

(H) Hematoxylin and eosin (H&E) staining of mouse lungs ($N = 6$ mice/group) at 18 h post-administration of EVs from infected or PBS-treated mice. Mice treated with EVs from T4-infected mice showed tissue microlesions (MLEs) and immune cell infiltration in the alveolar interstitium indicative of PLY-induced tissue damage (magnified in the inset). BR, bronchiole; MLE, microlesions. Scale bars, 200 μm. Blind histopathological scoring was performed based on presence or absence of cellularity in alveolar interstitium and lesions. A score of "0" was given when no lesions were found, and a score of "1" was given to tissue showing increasing cellularity and lesions. Mouse BALF flow cytometry and histology data are representative of three independent experiments. All data are represented as mean ± SEM. See also Figure S12.

termed as cross-dressing.[26,45] Importantly, we found that the trigger for EV shedding was only induced by the active toxin, but not the toxoid mutant PLYW433F, implying that cells sense a functional pore and respond by upregulating EV shedding. In this context, a recent study has shown that EVs released by cells intoxicated with cholesterol binding toxins are abundant in membrane repair proteins such as Copine-1 and Copine-3, indicating that membrane damage induces EV release.[46]

Our results indicated that EVs isolated from PLY-challenged cells had relatively smaller particle size compared to naive EVs. In agreement with our findings, Emerson et al.[47] recently reported a significant size reduction in EVs shed from *Salmonella*-infected macrophages compared to untreated cells. The biological significance of the smaller size of EVs from intoxicated cells needs further investigation in future studies.

Proteomic analysis of the PLY-EV cargo revealed the enrichment of key proteins involved in innate immune response and inflammation such as the gamma-interferon-inducible protein, IFI16; long pentraxin-related PTX3; the nucleotide-binding oligomerization domain (Nod)-like receptor, NLRC4; matrix metalloproteinase, MMP9; and superoxide dismutase, SOD2. The long pentraxin PTX3 is a complement-regulating protein that was reported to be upregulated upon pneumococcal infection.[48] Besides, we also found the presence of the matrix metalloproteinase MMP-9 specifically in PLY-EVs. PLY has been reported to promote MMP release from neutrophils that plays an important role in the progression of severe pneumococcal disease.[49] PLY is known to trigger oxidative stress,[50] hence it is conceivable that EVs contain superoxide dismutase to protect recipient cells from oxidative damage. Our findings are in agreement with Letsiou et al.[51] that found microvesicles released from lung epithelial cells to contain mitochondrial cargo and suppress neutrophil oxidative burst. Through oxidative damage, PLY also induces DNA double-strand breaks and results in the noncanonical histone H2 phosphorylation at the Ser-129 residue (H2AX). In agreement, we found that PLY-EVs contain the modified histone, H2AX. Our results suggest that PLY induces DNA double-strand breaks and cells get rid of damaged DNA through vesicles to maintain cellular homeostasis, consistent with Takahashi et al., 2017.[32] Besides, we identified several other histones, H2B, H3, and H4, to be significantly enriched in PLY-EVs, relative to naive EVs. Recently, mammalian histones have shown to exhibit synergy with antimicrobial peptides such as LL-37, by affecting bacterial membrane stability and inhibiting transcription,[52] suggesting that the PLY-induced EVs could be bactericidal. Taken together, our results suggest that EVs released from host cells harbor potential damage-associated molecular pattern molecules, which may serve to alert the host of infection and mount an anti-microbial and inflammatory response. Further studies are necessary to determine the effects of host-EVs on bacterial clearance by the host immune system.

Upon internalization by target cells, EVs deliver the cargo to the recipient cells. We found that PLY-EVs were better internalized by THP-1-monocyte-derived DCs as compared to naive EVs. This could be explained by studies showing PLY-induced endocytosis via MRC-1 receptor[53] in DCs and dynamin-dependent endocytosis in glial cells.[17] Upon internalization, the PLY-EVs induced DC maturation, consistent with the upregulation of costimulatory molecules and maturation markers. Naive EVs shed from untreated cells were also internalized but did not induce DC activation, supporting the notion that exosome-derived self-peptides maintain peripheral tolerance.[54] Importantly, pre-treatment of monocyte-derived DCs with PLY-EVs elicited higher inflammatory cytokine response upon infection with *S. pneumoniae*, compared to naive EVs. This suggests that the EV-associated PLY activates bystander cells for a robust response against subsequent infections. We also verified the immunostimulatory effect of PLY-EVs during infection using *S. pneumoniae*, T4R strain, as well as the isogenic PLY mutant strain, T4RΔply. Our data prompt us to speculate that EVs shed in response to bacterial toxin may elicit protection against infection due to their ability to prime DC responses. It also remains intriguing whether the EVs harbor MHC-bound antigens and directly activate T cells in the lymph nodes, in an APC-independent manner.

Using two *in vivo* models, zebrafish and mice, we demonstrated that PLY-EVs induce toxicity and inflammation. Zebrafish embryos administered with PLY-EVs showed severe pericardial edema, impaired heart function, and reduced overall survival compared to naive EVs. Circulating PLY has been shown to induce cardiac injury during pneumococcal infection.[55,56] Our study identifies a previously unrecognized mechanism for exacerbation of toxicity through EVs shed from PLY-challenged host cells. Using a PLY-induced acute lung injury mice model, we showed that EVs isolated from the lungs of treated mice induced inflammation when transferred to healthy recipients. Using an intranasal challenge mouse model, we found that infection with the wild-type serotype 4 pneumococcal strain T4 elicited higher EV release in the lungs,

when compared to the isogenic PLY mutant strain. This is in agreement with our hypothesis that the pore-forming toxin drives EV shedding from host cells. Adoptive transfer of EVs isolated from BALF of T4-, but not the T4Δply-, infected mice recapitulated the cytopathic effects of the toxin in healthy recipient mice. However, future studies are needed to investigate whether the EVs shed during infection could cause systemic effects.

Overall, our study proposes a mechanism by which host vesicles shed in response to bacterial toxins drive toxicity and inflammation. Our findings shed light on the role of host-derived vesicles during pneumococcal pathogenesis and their potential applications in EV-based diagnostic platforms using patient biopsies and biofluids such as lavage, blood, saliva, and urine. Future studies are required to fully characterize the other bacterial proteins in the shed host-EVs and their significance during infection.

Limitations of the study

A limitation of the study is that the effects of infection-induced host EVs *in vivo* were examined at early time point of 18 h and analyzed neutrophils and macrophages. Further studies are needed to examine the role of host EVs at later time points during infection on the activation of dendritic cells and T cells.

STAR★METHODS

Detailed methods are provided in the online version of this paper and include the following:

- KEY RESOURCES TABLE
- RESOURCE AVAILABILITY
  - Lead contact
  - Materials availability
  - Data and code availability
- EXPERIMENTAL MODEL AND STUDY PARTICIPANT DETAILS
  - Animals
  - Human material
  - Cell lines and primary cultures
- METHOD DETAILS
  - Cell culture
  - Primary monocyte isolation
  - Bacterial cultures and infection
  - Recombinant pneumolysin production
  - Endotoxin testing of recombinant pneumolysin
  - Isolation of EVs from cell cultures
  - Live-imaging of EV shedding from cells
  - Zeta potential and NTA analysis
  - Immunogold TEM analysis
  - Immunoblotting for EV markers and PLY
  - Quantification of PLY in EVs by densitometry
  - Hemolysis assay
  - PLY-CF647 conjugation and labeling of EVs
  - CFSE labeling of EVs and DC internalization
  - Mass spectrometry and data analysis
  - Flow cytometry of EV uptake and DC maturation
  - Cytokine ELISA
  - Zebrafish maintenance and EV microinjection
  - Zebrafish heartbeat, survival and qPCR
  - Intranasal PLY challenge and EV isolation
  - Mouse infection and adoptive transfer of EVs
- QUANTIFICATION AND STATISTICAL ANALYSIS

SUPPLEMENTAL INFORMATION

Supplemental information can be found online at https://doi.org/10.1016/j.isci.2024.110589.

ACKNOWLEDGMENTS

The study was supported by extramural funding through the INSPIRE Faculty fellowship Department of Science and Technology (DST/INSPIRE/04/2019/002238), Start-up grant (SRG/2021/000401) from the Science and Engineering Research Board (SERB), Ramalingaswami

Re-entry fellowship (BT/RLF/Re-entry/46/2020) from the Department of Biotechnology, India, and intramural funding from Rajiv Gandhi Centre for Biotechnology, Thiruvananthapuram. We extensively thank Prof. Birgitta Henriques Normark, Karolinska Institutet, Stockholm for sharing the pneumococcal strains used in the study. We thank the veterinary medical officers, Dr. Arya Aravind and Dr. Archana at the animal research facility, RGCB for technical assistance with mouse experiments. We thank pathologist, Dr. Krithiga K, Bioscience Research and Training Center, Thiruvananthapuram for histopathological examination. We acknowledge Prof. N. Sandhyarani, Department of Materials Science and Engineering National Institute of Technology, Calicut for the endotoxin measurement assays in recombinant protein samples. We thank Dr. K.C Sivakumar, Bioinformatics facility, RGCB for the proteomics data analysis. The technical assistance provided by Bindu Asokan, Rintu Varghese at the TEM facility, as well as Viji S at histology and Surabhi SV at the Bioimaging facility, RGCB is also acknowledged. Graphical abstract was created with BioRender.com.

AUTHOR CONTRIBUTIONS

K.S. conceptualized the project. K.S., S.P., C.V.B., S.D., S.S., Kuldeep. S., S.R., J.B.J., U.N., and A.B. developed the methodology. K.S., J.B.J., U.N., and A.B. acquired resources. K.S., S.P., C.V.B., A.C.S., S.A., A.J., A.D., S.D., S.S., Kuldeep. S., S.R., and J.B.J. conducted the investigations. K.S., S.P., C.V.B., A.C.S., A.J., S.A., S.D., S.S., J.B.J., and U.N. analyzed the data. K.S. wrote the original draft. K.S., J.B.J., U.N., and A.B. reviewed and edited the manuscript. K.S., J.B.J., U.N., and A.B. acquired funding. K.S., J.B.J., U.N., and A.B. supervised the project. All authors have reviewed and approved the manuscript.

DECLARATION OF INTERESTS

The authors declare no competing interests.

Received: February 2, 2024
Revised: June 11, 2024
Accepted: July 23, 2024
Published: July 25, 2024

REFERENCES

1. GBD 2016 Lower Respiratory Infections Collaborators (2018). Estimates of the global, regional, and national morbidity, mortality, and aetiologies of lower respiratory infections in 195 countries, 1990-2016: a systematic analysis for the Global Burden of Disease Study 2016. Lancet Infect. Dis. *18*, 1191–1210. https://doi.org/10.1016/S1473-3099(18)30310-4.
2. McAllister, D.A., Liu, L., Shi, T., Chu, Y., Reed, C., Burrows, J., Adeloye, D., Rudan, I., Black, R.E., Campbell, H., and Nair, H. (2019). Global, regional, and national estimates of pneumonia morbidity and mortality in children younger than 5 years between 2000 and 2015: a systematic analysis. Lancet Global Health *7*, e47–e57. https://doi.org/10.1016/S2214-109X(18)30408-X.
3. GBD 2019 Antimicrobial Resistance Collaborators (2022). Global mortality associated with 33 bacterial pathogens in 2019: a systematic analysis for the Global Burden of Disease Study 2019. Lancet *400*, 2221–2248. https://doi.org/10.1016/S0140-6736(22)02185-7.
4. Yahiaoui, R.Y., den Heijer, C.D., van Bijnen, E.M., Paget, W.J., Pringle, M., Goossens, H., Bruggeman, C.A., Schellevis, F.G., and Stobberingh, E.E.; APRES Study Team (2016). Prevalence and antibiotic resistance of commensal Streptococcus pneumoniae in nine European countries. Future Microbiol. *11*, 737–744. https://doi.org/10.2217/fmb-2015-0011.
5. Cherazard, R., Epstein, M., Doan, T.L., Salim, T., Bharti, S., and Smith, M.A. (2017). Antimicrobial Resistant Streptococcus pneumoniae: Prevalence, Mechanisms, and Clinical Implications. Am. J. Therapeut. *24*, e361–e369. https://doi.org/10.1097/MJT.0000000000000551.
6. Daniels, C.C., Rogers, P.D., and Shelton, C.M. (2016). A Review of Pneumococcal Vaccines: Current Polysaccharide Vaccine Recommendations and Future Protein Antigens. J. Pediatr. Pharmacol. Therapeut. *21*, 27–35. https://doi.org/10.5863/1551-6776-21.1.27.
7. Choe, Y.J., Lee, H.J., Lee, H., Oh, C.E., Cho, E.Y., Choi, J.H., Kang, H.M., Yoon, I.A., Jung, H.J., and Choi, E.H. (2016). Emergence of antibiotic-resistant non-vaccine serotype pneumococci in nasopharyngeal carriage in children after the use of extended-valency pneumococcal conjugate vaccines in Korea. Vaccine *34*, 4771–4776. https://doi.org/10.1016/j.vaccine.2016.08.030.
8. Weiser, J.N., Ferreira, D.M., and Paton, J.C. (2018). Streptococcus pneumoniae: transmission, colonization and invasion. Nat. Rev. Microbiol. *16*, 355–367. https://doi.org/10.1038/s41579-018-0001-8.
9. Nishimoto, A.T., Rosch, J.W., and Tuomanen, E.I. (2020). Pneumolysin: Pathogenesis and Therapeutic Target. Front. Microbiol. *11*, 1543. https://doi.org/10.3389/fmicb.2020.01543.
10. Pereira, J.M., Xu, S., Leong, J.M., and Sousa, S. (2022). The Yin and Yang of Pneumolysin During Pneumococcal Infection. Front. Immunol. *13*, 878244. https://doi.org/10.3389/fimmu.2022.878244.
11. Marshall, J.E., Faraj, B.H.A., Gingras, A.R., Lonnen, R., Sheikh, M.A., El-Mezgueldi, M., Moody, P.C.E., Andrew, P.W., and Wallis, R. (2015). The Crystal Structure of Pneumolysin at 2.0 A Resolution Reveals the Molecular Packing of the Pre-pore Complex. Sci. Rep. *5*, 13293. https://doi.org/10.1038/srep13293.
12. Tilley, S.J., Orlova, E.V., Gilbert, R.J.C., Andrew, P.W., and Saibil, H.R. (2005). Structural basis of pore formation by the bacterial toxin pneumolysin. Cell *121*, 247–256. https://doi.org/10.1016/j.cell.2005.02.033.
13. Mitchell, T.J., and Dalziel, C.E. (2014). The biology of pneumolysin. Subcell. Biochem. *80*, 145–160. https://doi.org/10.1007/978-94-017-8881-6_8.
14. Wolfmeier, H., Radecke, J., Schoenauer, R., Koeffel, R., Babiychuk, V.S., Drücker, P., Hathaway, L.J., Mitchell, T.J., Zuber, B., Draeger, A., and Babiychuk, E.B. (2016). Active release of pneumolysin prepores and pores by mammalian cells undergoing a Streptococcus pneumoniae attack. Biochim. Biophys. Acta *1860*, 2498–2509. https://doi.org/10.1016/j.bbagen.2016.07.022.
15. Babiychuk, E.B., and Draeger, A. (2015). Defying death: Cellular survival strategies following plasmalemmal injury by bacterial toxins. Semin. Cell Dev. Biol. *45*, 39–47. https://doi.org/10.1016/j.semcdb.2015.10.016.
16. Larpin, Y., Besançon, H., Iacovache, M.I., Babiychuk, V.S., Babiychuk, E.B., Zuber, B., Draeger, A., and Köffel, R. (2020). Bacterial pore-forming toxin pneumolysin: Cell membrane structure and microvesicle shedding capacity determines differential survival of cell types. FASEB J. *34*, 1665–1678. https://doi.org/10.1096/fj.201901737RR.
17. Hupp, S., Förtsch, C., Graber, F., Mitchell, T.J., and Iliev, A.I. (2022). Pneumolysin boosts the neuroinflammatory response to Streptococcus pneumoniae through enhanced endocytosis. Nat. Commun. *13*, 5032. https://doi.org/10.1038/s41467-022-32624-2.
18. Idone, V., Tam, C., Goss, J.W., Toomre, D., Pypaert, M., and Andrews, N.W. (2008). Repair of injured plasma membrane by rapid Ca2+-dependent endocytosis. J. Cell Biol.

180, 905–914. https://doi.org/10.1083/jcb.200708010.

19. Schorey, J.S., Cheng, Y., Singh, P.P., and Smith, V.L. (2015). Exosomes and other extracellular vesicles in host-pathogen interactions. EMBO Rep. *16*, 24–43. https://doi.org/10.15252/embr.201439363.
20. EL Andaloussi, S., Mäger, I., Breakefield, X.O., and Wood, M.J.A. (2013). Extracellular vesicles: biology and emerging therapeutic opportunities. Nat. Rev. Drug Discov. *12*, 347–357. https://doi.org/10.1038/nrd3978.
21. Bobrie, A., Colombo, M., Raposo, G., and Théry, C. (2011). Exosome secretion: molecular mechanisms and roles in immune responses. Traffic *12*, 1659–1668. https://doi.org/10.1111/j.1600-0854.2011.01225.x.
22. Muralidharan-Chari, V., Clancy, J., Plou, C., Romao, M., Chavrier, P., Raposo, G., and D'Souza-Schorey, C. (2009). ARF6-regulated shedding of tumor cell-derived plasma membrane microvesicles. Curr. Biol. *19*, 1875–1885. https://doi.org/10.1016/j.cub.2009.09.059.
23. Köffel, R., Wolfmeier, H., Larpin, Y., Besancon, H., Schoenauer, R., Babiychuk, V.S., Drucker, P., Pabst, T., Mitchell, T.J., Babiychuk, E.B., and Draeger, A. (2018). Host-Derived Microvesicles Carrying Bacterial Pore-Forming Toxins Deliver Signals to Macrophages: A Novel Mechanism of Shaping Immune Responses. Front. Immunol. *9*, 1688. https://doi.org/10.3389/fimmu.2018.01688.
24. Mir, B., and Goettsch, C. (2020). Extracellular Vesicles as Delivery Vehicles of Specific Cellular Cargo. Cells *9*, 1601. https://doi.org/10.3390/cells9071601.
25. Rossjohn, J., Gilbert, R.J., Crane, D., Morgan, P.J., Mitchell, T.J., Rowe, A.J., Andrew, P.W., Paton, J.C., Tweten, R.K., and Parker, M.W. (1998). The molecular mechanism of pneumolysin, a virulence factor from Streptococcus pneumoniae. J. Mol. Biol. *284*, 449–461. https://doi.org/10.1006/jmbi.1998.2167.
26. Prada, I., and Meldolesi, J. (2016). Binding and Fusion of Extracellular Vesicles to the Plasma Membrane of Their Cell Targets. Int. J. Mol. Sci. *17*, 1296. https://doi.org/10.3390/ijms17081296.
27. Rai, P., He, F., Kwang, J., Engelward, B.P., and Chow, V.T.K. (2016). Pneumococcal Pneumolysin Induces DNA Damage and Cell Cycle Arrest. Sci. Rep. *6*, 22972. https://doi.org/10.1038/srep22972.
28. Cotta-Ramusino, C., McDonald, E.R., 3rd, Hurov, K., Sowa, M.E., Harper, J.W., and Elledge, S.J. (2011). A DNA damage response screen identifies RHINO, a 9-1-1 and TopBP1 interacting protein required for ATR signaling. Science *332*, 1313–1317. https://doi.org/10.1126/science.1203430.
29. Gomez, V., Gundogdu, R., Gomez, M., Hoa, L., Panchal, N., O'Driscoll, M., and Hergovich, A. (2015). Regulation of DNA damage responses and cell cycle progression by hMOB2. Cell. Signal. *27*, 326–339. https://doi.org/10.1016/j.cellsig.2014.11.016.
30. Ye, X., Ong, N., An, H., and Zheng, Y. (2020). The Emerging Roles of NDR1/2 in Infection and Inflammation. Front. Immunol. *11*, 534. https://doi.org/10.3389/fimmu.2020.00534.
31. Simpson, R.J., Jensen, S.S., and Lim, J.W.E. (2008). Proteomic profiling of exosomes: current perspectives. Proteomics *8*, 4083–4099. https://doi.org/10.1002/pmic.200800109.
32. Takahashi, A., Okada, R., Nagao, K., Kawamata, Y., Hanyu, A., Yoshimoto, S., Takasugi, M., Watanabe, S., Kanemaki, M.T., Obuse, C., and Hara, E. (2017). Exosomes maintain cellular homeostasis by excreting harmful DNA from cells. Nat. Commun. *8*, 15287. https://doi.org/10.1038/ncomms15287.
33. Morita, S., Tagai, C., Shiraishi, T., Miyaji, K., and Iwamuro, S. (2013). Differential mode of antimicrobial actions of arginine-rich and lysine-rich histones against Gram-positive Staphylococcus aureus. Peptides *48*, 75–82. https://doi.org/10.1016/j.peptides.2013.07.025.
34. Gomes, M.C., and Mostowy, S. (2020). The Case for Modeling Human Infection in Zebrafish. Trends Microbiol. *28*, 10–18. https://doi.org/10.1016/j.tim.2019.08.005.
35. Subramanian, K., Iovino, F., Tsikourkitoudi, V., Merkl, P., Ahmed, S., Berry, S.B., Aschtgen, M.S., Svensson, M., Bergman, P., Sotiriou, G.A., and Henriques-Normark, B. (2020). Mannose receptor-derived peptides neutralize pore-forming toxins and reduce inflammation and development of pneumococcal disease. EMBO Mol. Med. *12*, e12695. https://doi.org/10.15252/emmm.202012695.
36. Jim, K.K., Engelen-Lee, J., van der Sar, A.M., Bitter, W., Brouwer, M.C., van der Ende, A., Veening, J.W., van de Beek, D., and Vandenbroucke-Grauls, C.M.J.E. (2016). Infection of zebrafish embryos with live fluorescent Streptococcus pneumoniae as a real-time pneumococcal meningitis model. J. Neuroinflammation *13*, 188. https://doi.org/10.1186/s12974-016-0655-y.
37. Witzenrath, M., Gutbier, B., Hocke, A.C., Schmeck, B., Hippenstiel, S., Berger, K., Mitchell, T.J., de los Toyos, J.R., Rosseau, S., Suttorp, N., and Schütte, H. (2006). Role of pneumolysin for the development of acute lung injury in pneumococcal pneumonia. Crit. Care Med. *34*, 1947–1954. https://doi.org/10.1097/01.CCM.0000220496.48295.A9.
38. Zafar, M.A., Wang, Y., Hamaguchi, S., and Weiser, J.N. (2017). Host-to-Host Transmission of Streptococcus pneumoniae Is Driven by Its Inflammatory Toxin, Pneumolysin. Cell Host Microbe *21*, 73–83. https://doi.org/10.1016/j.chom.2016.12.005.
39. Panagiotou, S., Chaguza, C., Yahya, R., Audshasai, T., Baltazar, M., Ressel, L., Khandaker, S., Alsahag, M., Mitchell, T.J., Prudhomme, M., et al. (2020). Hypervirulent pneumococcal serotype 1 harbours two pneumolysin variants with differential haemolytic activity. Sci. Rep. *10*, 17313. https://doi.org/10.1038/s41598-020-73454-w.
40. Wolfmeier, H., Schoenauer, R., Atanassoff, A.P., Neill, D.R., Kadioglu, A., Draeger, A., and Babiychuk, E.B. (2015). Ca^{2+}-dependent repair of pneumolysin pores: A new paradigm for host cellular defense against bacterial pore-forming toxins. Biochim. Biophys. Acta *1853*, 2045–2054. https://doi.org/10.1016/j.bbamcr.2014.09.005.
41. Besançon, H., Larpin, Y., Babiychuk, V.S., Koffel, R., and Babiychuk, E.B. (2022). Engineered Liposomes Protect Immortalized Immune Cells from Cytolysins Secreted by Group A and Group G Streptococci. Cells *11*, 166. https://doi.org/10.3390/cells11010166.
42. Fang, R.H., Luk, B.T., Hu, C.M.J., and Zhang, L. (2015). Engineered nanoparticles mimicking cell membranes for toxin neutralization. Adv. Drug Deliv. Rev. *90*, 69–80. https://doi.org/10.1016/j.addr.2015.04.001.
43. Henry, B.D., Neill, D.R., Becker, K.A., Gore, S., Bricio-Moreno, L., Ziobro, R., Edwards, M.J., Mühlemann, K., Steinmann, J., Kleuser, B., et al. (2015). Engineered liposomes sequester bacterial exotoxins and protect from severe invasive infections in mice. Nat. Biotechnol. *33*, 81–88. https://doi.org/10.1038/nbt.3037.
44. Antimisiaris, S.G., Mourtas, S., and Marazioti, A. (2018). Exosomes and Exosome-Inspired Vesicles for Targeted Drug Delivery. Pharmaceutics *10*, 218. https://doi.org/10.3390/pharmaceutics10040218.
45. Zeng, F., and Morelli, A.E. (2018). Extracellular vesicle-mediated MHC cross-dressing in immune homeostasis, transplantation, infectious diseases, and cancer. Semin. Immunopathol. *40*, 477–490. https://doi.org/10.1007/s00281-018-0679-8.
46. Alves, S., Pereira, J.M., Mayer, R.L., Gonçalves, A.D.A., Impens, F., Cabanes, D., and Sousa, S. (2022). Cells Responding to Closely Related Cholesterol-Dependent Cytolysins Release Extracellular Vesicles with a Common Proteomic Content Including Membrane Repair Proteins. Toxins *15*, 4. https://doi.org/10.3390/toxins15010004.
47. Emerson, L.E., Mosby, C.A., Enslow, S., Hui, W.W., Jones, M.K., and Ferraro, M.J. (2024). Changes in lipid composition of host-derived extracellular vesicles following Salmonella infection. Microbiol. Spectr. *12*, e0279623. https://doi.org/10.1128/spectrum.02796-23.
48. Koh, S.H., Shin, S.G., Andrade, M.J., Go, R.H., Park, S., Woo, C.H., and Lim, J.H. (2017). Long pentraxin PTX3 mediates acute inflammatory responses against pneumococcal infection. Biochem. Biophys. Res. Commun. *493*, 671–676. https://doi.org/10.1016/j.bbrc.2017.08.133.
49. Cockeran, R., Mitchell, T.J., Feldman, C., and Anderson, R. (2009). Pneumolysin induces release of matrix metalloproteinase-8 and -9 from human neutrophils. Eur. Respir. J. *34*, 1167–1170. https://doi.org/10.1183/09031936.00007109.
50. Martner, A., Dahlgren, C., Paton, J.C., and Wold, A.E. (2008). Pneumolysin released during Streptococcus pneumoniae autolysis is a potent activator of intracellular oxygen radical production in neutrophils. Infect. Immun. *76*, 4079–4087. https://doi.org/10.1128/IAI.01747-07.
51. Letsiou, E., Teixeira Alves, L.G., Fatykhova, D., Felten, M., Mitchell, T.J., Müller-Redetzky, H.C., Hocke, A.C., and Witzenrath, M. (2021). Microvesicles released from pneumolysin-stimulated lung epithelial cells carry mitochondrial cargo and suppress neutrophil oxidative burst. Sci. Rep. *11*, 9529. https://doi.org/10.1038/s41598-021-88897-y.
52. Doolin, T., Amir, H.M., Duong, L., Rosenzweig, R., Urban, L.A., Bosch, M., Pol, A., Gross, S.P., and Siryaporn, A. (2020). Mammalian histones facilitate antimicrobial synergy by disrupting the bacterial proton gradient and chromosome organization. Nat. Commun. *11*, 3888. https://doi.org/10.1038/s41467-020-17699-z.
53. Subramanian, K., Neill, D.R., Malak, H.A., Spelmink, L., Khandaker, S., Dalla Libera Marchiori, G., Dearing, E., Kirby, A., Yang, M., Achour, A., et al. (2019). Pneumolysin binds to the mannose receptor C type 1 (MRC-1) leading to anti-inflammatory responses and enhanced pneumococcal survival. Nat. Microbiol. *4*, 62–70. https://doi.org/10.1038/s41564-018-0280-x.

54. Morelli, A.E., Larregina, A.T., Shufesky, W.J., Sullivan, M.L.G., Stolz, D.B., Papworth, G.D., Zahorchak, A.F., Logar, A.J., Wang, Z., Watkins, S.C., et al. (2004). Endocytosis, intracellular sorting, and processing of exosomes by dendritic cells. Blood *104*, 3257–3266. https://doi.org/10.1182/blood-2004-03-0824.

55. Alhamdi, Y., Neill, D.R., Abrams, S.T., Malak, H.A., Yahya, R., Barrett-Jolley, R., Wang, G., Kadioglu, A., and Toh, C.H. (2015). Circulating Pneumolysin Is a Potent Inducer of Cardiac Injury during Pneumococcal Infection. PLoS Pathog. *11*, e1004836. https://doi.org/10.1371/journal.ppat.1004836.

56. Brown, A.O., Mann, B., Gao, G., Hankins, J.S., Humann, J., Giardina, J., Faverio, P., Restrepo, M.I., Halade, G.V., Mortensen, E.M., et al. (2014). Streptococcus pneumoniae translocates into the myocardium and forms unique microlesions that disrupt cardiac function. PLoS Pathog. *10*, e1004383. https://doi.org/10.1371/journal.ppat.1004383.

57. Littmann, M., Albiger, B., Frentzen, A., Normark, S., Henriques-Normark, B., and Plant, L. (2009). Streptococcus pneumoniae evades human dendritic cell surveillance by pneumolysin expression. EMBO Mol. Med. *1*, 211–222. https://doi.org/10.1002/emmm.200900025.

58. Surve, M.V., Bhutda, S., Datey, A., Anil, A., Rawat, S., Pushpakaran, A., Singh, D., Kim, K.S., Chakravortty, D., and Banerjee, A. (2018). Heterogeneity in pneumolysin expression governs the fate of Streptococcus pneumoniae during blood-brain barrier trafficking. PLoS Pathog. *14*, e1007168. https://doi.org/10.1371/journal.ppat.1007168.

59. Kuttoth, H., Thomas, T., Nair, R.V., and Sandhyarani, N. (2023). Label-free detection of endotoxin and gram-negative bacteria from water using copper (I) oxide anchored reduced graphene oxide. Anal. Chim. Acta *1237*, 340597. https://doi.org/10.1016/j.aca.2022.340597.

60. Perez-Riverol, Y., Bai, J., Bandla, C., García-Seisdedos, D., Hewapathirana, S., Kamatchinathan, S., Kundu, D.J., Prakash, A., Frericks-Zipper, A., Eisenacher, M., et al. (2022). The PRIDE database resources in 2022: a hub for mass spectrometry-based proteomics evidences. Nucleic Acids Res. *50*, D543–D552. https://doi.org/10.1093/nar/gkab1038.

61. Wick, M.J., Harral, J.W., Loomis, Z.L., and Dempsey, E.C. (2018). An Optimized Evans Blue Protocol to Assess Vascular Leak in the Mouse. J. Vis. Exp. *139*, 57037. https://doi.org/10.3791/57037.

STAR★METHODS

KEY RESOURCES TABLE

REAGENT or RESOURCE	SOURCE	IDENTIFIER
Antibodies		
Mouse anti-pneumolysin (PLY)	Abcam	Cat#ab71810; RRID: AB_1269828
Gold conjugated goat anti-mouse IgG	Jackson Immuno Research Laboratories	Cat#115-205-068; RRID: AB_2338730
Mouse anti-CD81	Abcam	Cat#ab79559; RRID: AB_1603682
Rabbit anti-CD63	Abcam	Cat#ab134045; RRID: AB_2800495
Rabbit anti-TSG101	Abcam	Cat#ab125011; RRID: AB_10974262
6x-His Tag Monoclonal antibody	Thermo Fisher Scientific	Cat #MA1-21315; RRID: AB_557403
HRP-conjugated anti-mouse IgG	Bio-Rad	Cat# 1706516; RRID: AB_2921252
HRP-conjugated anti-rabbit IgG	Bio-Rad	Cat# 1706515; RRID: AB_11125142
BD Pharmingen PE mouse antihuman-CD80	BD Biosciences	Cat#560925; RRID: AB_396606
PE-*anti*-human CD83	Biolegend	Cat#305327; RRID: AB_2564259
FITC Mouse anti-CD86	BD Biosciences	Cat#560958; RRID: AB_396012
PE anti-mouse Ly6G	Biolegend	Cat#127607; RRID: AB_1186104
FITC anti-mouse F4/80	Biolegend	Cat#123107; RRID: AB_893500
APC mouse anti-human CD 11c	BD Biosciences	Cat#560895; RRID: AB_398680
Ptx3 Antibody (C-10)-Mouse monoclonal antibody	Santa Cruz Biotechnology	Cat# sc-373951; RRID: AB_10920402
Mouse Anti-Human HCCA2 Monoclonal Antibody, Unconjugated, Clone 2400C3a (MOB2)	Santa Cruz Biotechnology	Cat# sc-81564; RRID: AB_2241891
HIST1H2BB Polyclonal Antibody	Thermo Fisher Scientific	Cat# PA5-117473; RRID: AB_2902103
Mouse Anti-Actin, beta Monoclonal Antibody, Unconjugated, Clone mAbcam 8226	Abcam	Cat# ab8226; RRID: AB_306371
Bacterial and virus strains		
Encapsulated *Streptococcus pneumoniae* serotype 4 strain TIGR4 Isogenic unencapsulated pneumococcal strain, T4R Isogenic pneumolysin (PLY) mutant pneumococcal strain,T4Δply PLY- mutant unencapsulated pneumococcal strain, T4RΔply	Prof. Birgitta Henriques Normark, Karolinska Institute, Stockholm	Littmann et al.[57]
Escherichia Coli BL21 (DE3)	Prof. Anirban Banerjee, Indian Institute of Technology Bombay	Surve et al.[58]
Biological samples		
Human blood for hemolysis and primary monocyte isolation	Healthy donors at Rajiv Gandhi Center for Biotechnology	N/A
Chemicals, peptides, and recombinant proteins		
Human GM-CSF	Peprotech	300-03-20UG
Human IL-4	Peprotech	200-04-20UG

(*Continued on next page*)

Continued

REAGENT or RESOURCE	SOURCE	IDENTIFIER
Human TNF-α	Peprotech	300-01A-10UG
Ionomycin	Sigma	0000116970
O.C.T. Compound	Tissue Tek Sakura	IA018
RPMI 1640 Medium	HiMedia	AL028A
Fetal Bovine Serum	Invitrogen	10270106
Dulbecco's Modified Eagle Medium	HiMedia	AL006A
Soyabean Casein digest agar with 5% sheep blood	HiMedia	M011-100G
Brain Heart Infusion broth	HiMedia	M210-500G
Recombinant His tagged pnemolysin (PLY) GFP-tagged pneumolysin (PLY) PLY-W33F toxoid mutant Recombinant Pneumolysin	Prof. Anirban Banerjee, IIT Bombay	Surve et al.[58]
Fixable Viability Dye eFluor 780	eBioscience	65-0865-14
MTT dye	Invitrogen	M6494
Dimethyl sulphoxide (DMSO)	HiMedia	GRM5856
Exoquick TC reagent	System Bioscience	EXOTC10A-1
Phosphate Buffered Saline(PBS)	HiMedia	TL1099
Nile red	Invitrogen	N1142
Vibrant DiI Cell Labeling solution	Thermo Fisher Scientific	V22885
Bovine Serum Albumin	HiMedia	TC546
Gentamycin	HiMedia	A005
Glutaraldehyde	Sigma	G6257
Uranyless stain	Electron Microscopy Sciences	22409
RIPA Lysis buffer	HiMedia	TCL131
Triton X-100	HiMedia	RM845-500ML
Mix-*n*-Stain CF647 labeling kit	Biotium	92449
4% Paraformaldehyde	HiMedia	TCL119
Prolong Gold antifade mounting medium with DAPI	Invitrogen	P36941
CFSE dye	Invitrogen	C34570 A
Rapigest SF	Waters	186001860
Iodoacetamide	Sigma Aldrich	Proteomics facility, Rajiv Gandhi Center for Biotechnology animal Facility
1,4 Dithiothreitol	Sigma Aldrich	
MS grade trypsin	Sigma Aldrich	
Cytochalasin D	Sigma Aldrich	C2618
Tricaine	Sigma Aldrich	E10521
Isofluorane	SOSRANE	KD/2691A
Evans blue	Sigma Aldrich	E2129-10G
EDTA	HiMedia	GRM3915-500G
RosetteSep Human Monocyte Enrichment Cocktail	Stem cell technologies	Cat#15068
Hematoxylin	HiMedia	S058
Eosin	HiMedia	GRM 1060

(*Continued on next page*)

Continued

REAGENT or RESOURCE	SOURCE	IDENTIFIER
HiSep™ LSM 1077	HiMedia	LS001
Ibidi mounting medium	Ibidi	50001
Precision protein western c standard	Bio-Rad	1610376
Precision Protein™ StrepTactin-HRP Conjugate	Bio-Rad	1610381
Clarity western ECL substrate	Bio-Rad	1705060
Transblot turbo 5X	Bio-Rad	10026938
4X Lamelli	Bio-Rad	1610747
Ammonium Persulphate	Bio-Rad	1610700
TEMED	Bio-Rad	1610806
SDS	Bio-Rad	1610301
Glycine	Bio-Rad	1610718
Ni-NTA agarose	Qiagen	30210
Imidazole reagent	HiMedia	MB019-100G
PD-10 buffer exchange column	GE Healthcare	17085101
Luria Bertani(LB) Media	HiMedia	M575-550G
Kanamycin	HiMedia	MB105-5G
IPTG	HiMedia	RM2578-10G
Critical commercial assays		
BCA protein assay	Thermo Scientific	23227
Human TNF-α DuoSet ELISA kit	R & D Systems	DY210-05
Human IL-12 DuoSet ELISA kit	R & D Systems	DY1270-05
Mouse TNF-α DuoSet ELISA kit	R & D Systems	DY410-05
Mouse IL-1 DuoSet ELISA kit	R & D Systems	DY401-05
HOT FIREPol® EvaGreen® qPCR Mix Plus	SOLIS BIODYNE	08-24-0000S
Deposited data		
Proteomics raw data	This paper	ProteomeXchange Consortium (PRIDE): PXD052436. https://doi.org/10.6019/PXD052436
Raw data and analysis files, deposited in Mendeley Data	This paper	Mendeley Data: https://doi.org/10.17632/h766k7nyc4.1
Experimental models: Cell lines		
Human monocytic leukemia cell line, THP-1	National Center for Cell Sciences, Pune, India	ATCC TIB-202
Human adenocarcinomic alveolar basal epithelial cells, A549	National Center for Cell Sciences, Pune, India	ATCC CCL-185
Experimental models: Organisms/strains		
Danio rerio	Local vendors in Banglore	Maintained at DBGL Zebrafish Facility Center, Indian Institute of Science, Bangalore
C57BL/6J	Animal Research Facility, Rajiv Gandhi Center for Biotechnology animal Facility	Bred in-house
Oligonucleotides		
ply-NdeI-F Sigma 5′-GACGTAGGCATATG ATGGCAAATAAAGCAGT-3′		

(*Continued on next page*)

Continued

REAGENT or RESOURCE	SOURCE	IDENTIFIER
ply-XhoI-R 5′-GTGTGTCTCGAGCTAG TCATTTTCTACCTTAT-3′	Sigma	
ply-F-W433F 5′-GAGAGTGTACCGGGTTGC CTTTGAATGGTGGCGTACGGTTTA-3′		
ply-R-W433F 5′-TAAACCGTACGCCACCATT CAAAGGCAAGCCCGGTACACTCTC-3′		
GFP-PLY Nco1-F 5′-GACTAACTCCATG GCAAAAGGAGAAGAGCTGTTCACAG-3′		
GFP-PLY-Xho1-R 5′-ATAATGCTCGA GGTCATTTTCTACCTTATCCTCTACCTG-3′		
TNF-α Forward Primer- 5′- GGAGAGTTGCC TTTACCGCT-3′		
TNF-α Reverse Primer- 5′- GATTGCCCTGGG TCTTAGGAG-3′		
β-actin (Forward Primer: 5′- CACTGAGGC TCCCCTGAATCCC-3′,		
β-actin Reverse Primer: 5′- CGTACAGAGAGA GCACAGCCTGG-3′		
Recombinant DNA		
pAB400 (6XHis-Ply in pET28a)	Cloned in the Anirban lab, IITB	
pAB422 (6XHis-GFP-Ply in pET28a)	Cloned in the Anirban lab, IITB	
pAB044	Cloned in the Anirban lab, IITB	
Software and algorithms		
Microsoft Office Excel	Microsoft	https://www.microsoft.com
Microsoft Office Powerpoint	Microsoft	https://www.microsoft.com
FACS Diva	BD Life Sciences	v9.0
FlowJo	BD Life Sciences	v10.8
Leica LASX		https://www.leica-microsystems.com/products/microscope-software/p/leica-las-x-ls/
ImageJ version 1.53		https://imagej.net/ij/
Progenesis QI for proteomics v4.2		https://www.nonlinear.com/progenesis/qi-for-proteomics/v4.2/
Bioinformatics and Evolutionary Genomics		http://bioinformatics.psb.ugent.be/webtools/Venn/
DESEQ2 (R software)		https://bioconductor.org/packages/release/bioc/html/DESeq2.html
gprofiler		https://biit.cs.ut.ee/gprofiler/gost
GraphPad Prism V.9.12		https://www.graphpad.com/
Biorender		https://www.biorender.com/
Adobe Illustrator		https://www.adobe.com/in/products/illustrator.html
Other		
Amicon® Ultra Centrifugal Filter, 100 kDa MWCO (4 mL)	Sigma Aldrich	UFC810024
Amicon® Ultra Centrifugal Filter, 100 kDa MWCO (0.5 mL)	Sigma Aldrich	UFC510096

(*Continued on next page*)

Continued

REAGENT or RESOURCE	SOURCE	IDENTIFIER
Formvar-coated copper grid	Electron microscopic Sciences	FCF400-Cu
PVDF membrane	Bio-Rad	1620177
0.45 μm syringe driven filter	HiMedia	SF144
0.22 μm syringe driven filter	HiMedia	SF143
Exocarta		http://www.exocarta.org/
Vesiclepedia		http://www.microvesicles.org/
String database		https://string-db.org/

RESOURCE AVAILABILITY

Lead contact

Further information and requests for resources and reagents should be directed to and will be fulfilled by the lead contact, Dr. Karthik Subramanian karthik@rgcb.res.in.

Materials availability

This study did not generate new unique reagents.

Data and code availability

- The proteomics data have been deposited to the ProteomeXchange Consortium with accession PXD052436 and are publicly available as of the date of publication. The raw data and analysis files associated with this study are deposited in Mendeley Data and are publicly available as of the date of publication. The DOI is listed in the key resources table.
- This paper does not report original code.
- Any additional information required to reanalyse the data reported in this paper is available from the lead contact upon request.

EXPERIMENTAL MODEL AND STUDY PARTICIPANT DETAILS

Animals

The zebrafish study was approved by the Institutional animal ethical committee, Indian Institute of Science, Bangalore (Ref. CAF/ETHICS/965/2023). Adult healthy wild-type zebrafish (Danio rerio) were procured from local vendors in Bangalore, India. Zebrafish were maintained in DBGL Zebrafish Facility Center, Indian Institute of Science, Bangalore with continuous aeration with 14 h light/10 h darkness photoperiod and maintained at 28 $\pm$ 1°C. At least 60 embryos/group were used and randomly assigned to the groups.

Mouse experiments were approved by the institutional animal ethics committee (Ref. IAEC/896/KARTHIKS/2022). C57BL/6J mice were generated and maintained at the Animal Research Facility, RGCB using Individually Ventilated Caging system with 14 h light/10 h darkness at 25°C with *ad libitum* access to food and water. Mice were used at the age of 8–12 weeks. The mice were randomly assigned to the experimental groups and included minimum of 5 mice/group. The sample size was determined based on previous experience[35] and accounting the mortality rate.

Human material

Peripheral blood was collected from healthy donors (both male and female) by a trained phlebotomist upon obtaining informed consent and the study was approved by the Institutional human ethical committee, RGCB (Ref. IHEC/12/2020_E/14).

Cell lines and primary cultures

Human THP-1 monocytes (ATCC TIB-202) and alveolar basal epithelial cells A549 (ATCC CCL-185) cells were procured from the national cell repository at the National Center for Cell Science, Pune and are male. The cell lines were authenticated using short tandem repeat analysis and tested negative for mycoplasma contamination. Primary human monocytes were isolated from peripheral blood collected from healthy donors (male and female) at RGCB, Thiruvananthapuram upon obtaining informed consent. All cells were maintained at 37°C with 5% CO_2.

METHOD DETAILS

Cell culture

Human THP-1 monocytes were cultured in RPMI 1640 medium (HiMedia) supplemented with 10% fetal bovine serum (FBS) (Invitrogen). Human A549 cells were grown in DMEM (HiMedia) supplemented with 10% FBS. Cell cultures were maintained in 5% CO_2 at 37°C. THP-1 monocyte-derived DCs were differentiated by stimulating THP-1 cells with human GMCSF (1500 IU/mL) and IL-4 (1500 IU/mL) (Peprotech) for 5 days

with half the medium replaced at day 3. To induce maturation, TNF-α (2000 IU/mL, Peprotech) and Ionomycin (200 ng/mL) was added at day 5 and further incubated for 2 days. The DCs were characterized and verified for surface expression of characteristics markers, CD80, CD86 and CD83 by flow cytometry (Figure S6).

Primary monocyte isolation

Human primary monocytes were isolated from 30 mL of pooled donor blood (10 mL/donor) collected in EDTA Vacutainer tubes (BD Biosciences) from three independent, healthy donors. Informed consent was obtained in accordance with the ethical approved protocol (Ref. IHEC/12/2020_E/14). Rosettesep human monocyte enrichment cocktail (Stem Cell Technologies) was added at 50 μL/mL blood and incubated for 20 min at room temperature. An equal volume of recommended media (2% FBS and 1 mM EDTA in PBS) was added and carefully layered over the HiSep LSM 1073 density gradient medium (HiMedia) at 15 mL for 20 mL diluted whole blood. The tubes were then centrifuged at 1200 g for 20 min with brakes off. The white buffy layer containing the primary monocytes was carefully collected, topped with recommended media, and centrifuged at 300 g for 10 min with low brakes. The cell pellet was topped up using the recommended media followed by centrifugation at 120 × *g* for 10 min to remove the platelets. The washes were repeated six times with recommended media and pelleted at 300 g for 10 min. The primary monocytes were then resuspended in DC differentiation medium consisting of RPMI supplemented with 40 ng/mL of human recombinant GM-CSF (Peprotech) and IL-4 (Peprotech) and maintained in 5% CO_2, at 37°C.

Bacterial cultures and infection

The encapsulated *S. pneumoniae* serotype 4 strain TIGR4 (T4; ATCC BAA-334) and the unencapsulated strain, T4R, and their respective isogenic PLY-deficient mutant strains, T4Δply and T4RΔply used in this study[57] are a kind gift from Prof. Birgitta Henriques Normark, Karolinska Institutet, Stockholm. The strains were grown overnight on soyabean casein digest agar plates with 5% sheep blood (HiMedia) in 5% CO_2 at 37°C. For infection, liquid cultures were grown in brain heart infusion broth (HiMedia) at 37°C to OD of 0.4 and pelleted at 5000 rpm for 5 min. All infection experiments were performed with prior approval from the Institutional biosafety committee, RGCB (ref. 51/IBSC/karthik/202151) and Review Committee on Genetic Manipulation, Department of Biotechnology, Govt. of India (Ref. BT/IBKP/363/2020).

Recombinant pneumolysin production

The gene encoding Ply was amplified from *S. pneumoniae* TIGR4 genomic DNA with primers, ply-NdeI-F and ply-XhoI-R (Forward Primer: 5′-GACGTAGGCATATGATGGCAAATAAAGCAGT-3′) (Reverse Primer: 5′-GTGTGTCTCGAGCTAGTCATTTTCTACCTTAT-3′) and cloned between Nde1 and Xho1 sites in the pET28a vector. The ply W433F variant was created by site-directed mutagenesis in wild-type ply using primers ply-F-W433F and ply-R-W433F (Forward Primer: 5′- GAGAGTGTACCGGGTTGCCTTTGAATGGTGGCGTACGGTTTA-3′) (Reverse Primer: 5′- TAAACCGTACGCCACCATTCAAAGGCAAGCCCGGTACACTCTC-3′). For the 6X His-tagged GFP-PLY fusion protein, the *gfp* and *ply* genes were joined together by the overlap PCR method and the chimeric gene fragment was cloned in the plasmid pAB044 among Xho1 and BamH1 site now named pAB404. Further, the *gfp-linker-ply* fragment was amplified from pAB404 using primers i.e., GFP-PLY Nco1-F (Forward Primer: 5′- GACTAACTCCATGGCAAAAGGAGAAGAGCTGTTCACAG-3′) and GFP-PLY-Xho1-R (Reverse Primer: 5′-ATAATGCTCGAGGTCATTTTCTACCTTATCCTCTACCTG-3′) and cloned between Nco1 and Xho1 sites in the pET28a vector. All constructs were verified by DNA sequencing. The recombinant plasmids were transformed in the *E. coli* BL21 (DE3) strain for protein overexpression. Freshly transformed colonies were grown in Luria-Bertani (LB) media containing 50 μg/mL kanamycin at 37°C at 180 rpm for 12 h in a shaker incubator. The 1% of the primary culture was inoculated in the fresh 1L of LB media containing 50 μg/mL kanamycin and incubated at 37°C at 180 rpm till $O.D._{600}$ = 0.8 was achieved. The protein expression was induced by adding 400 μM IPTG in the culture and allowed further growth at 22°C at 180 rpm for 4–5 h. The cells were harvested by centrifugation at 10000 rpm for 10 min at 4°C. The cell pellet was resuspended in lysis buffer (50 mM Tris pH 8.0, 300 mM NaCl, 1 mM PMSF and 5 mM beta-mercaptoethanol) and sonicated at 50% amplitude, pulse 20 s on and 20 s off for the lysis of the cells. The cell debris was removed by centrifugation at 15000 rpm for 45 min at 4°C. The cell lysate was filtered through 0.22 μm filters and loaded on the Ni-NTA column pre-equilibrated with equilibration buffer (50 mM Tris pH 8.0, 300 mM NaCl). The column was washed with 10 volumes of equilibration buffer. Non-specific and loosely bound proteins were removed by running a linear imidazole gradient ranging from 30 to 90 mM in the equilibration buffer. Finally, the 6X-His-tagged proteins were eluted by the elution buffer (50 mM Tris pH 8.0, 300 mM NaCl, 250 mM imidazole) from the column. The purity of the proteins was confirmed by SDS-PAGE analysis. The fractions were pooled and concentrated up to 2 mg/mL using 10 kDa molecular weight cut-off filter by centrifugation at 4000 rpm at 4°C. The elution buffer was exchanged to the reaction buffer (25 mM Tris pH 7.5, 250 mM NaCl) by performing buffer exchange using PD-10 buffer exchange columns. The purified recombinant PLY-His and PLY-GFP proteins were verified by hemolysis assay to have comparable lytic activity (Figure S4A).

Endotoxin testing of recombinant pneumolysin

The sensor surface PmB/rGO-Cu_2O/GCE was prepared as described previously[59] and endotoxin detection was carried out with differential pulse voltammetry. A linear response in change in peak current with the increasing concentrations of endotoxin was obtained. The corresponding calibration plot was obtained with an R^2 value of 0.995 in the concentration range of 10 ag/mL to 100 pg/mL. To detect the endotoxin level in the unknown samples, first DPV measurement of the bare sensor PmB/rGO-Cu_2O/GCE was done in a three electrode setup with

PBS as the electrolyte solution. Then to this 10 mL of PBS, 10 μL of the sample solution was added, stirred the solution for 1 min and again the differential pulse voltammetry experiment was conducted. The change in peak current on addition of the sample, compared to the bare sensor surface was calculated from the differential pulse voltammograms and the endotoxin concentration was found from the calibration plot. The endotoxin level in toxoid mutant PLYW33F was calculated to be 0.3 fg/mL and a very low response was obtained for wild type PLY, which implies the absence of endotoxin in the sample or below detection limit of 10 ag/mL.

Isolation of EVs from cell cultures

To pre-deplete serum-derived exosomes, FBS supplemented RPMI medium was centrifuged at 100,000 g overnight and passed through 0.2-μm filter. For isolation of PLY-EVs, 6 × 10^7 THP-1 monocytes were stimulated with 0.1 μg/mL and 0.5 μg/mL of purified recombinant His-tagged PLY, GFP-tagged PLY or the toxoid mutant, PLYW433F in EV-depleted medium for 24 h at 37°C. Untreated cells served as negative control. Recombinant PLY-WT and PLYW433F toxoid proteins were recombinantly expressed in *E. coli* BL21 (DE3) and purified as described previously[58] by Prof. Anirban Banerjee, Indian Institute of Technology Bombay. The percentage of dead cells was quantified by staining with the Fixable Viability Dye eFluor 780 (eBioscience, 1:50,000 dilution) following the manufacturer's protocol. For MTT cell viability assay, 10-fold serial dilutions from 1 × 10^6 to 1 × 10^3 cells/mL were incubated with 0.5 mg/mL MTT dye (Invitrogen) for 2 h, solubilized using 100 μL DMSO and MTT dye absorbance at 570 nm was measured using Varioskan LUX multimode microplate reader (ThermoFisher Scientific). For infection-induced EVs, cells were infected with *S. pneumoniae*, T4R or isogenic PLY mutant strain, T4RΔply in EV-depleted medium for 2 h at MOI of 10, following which the extracellular bacteria were removed by PBS washes and gentamicin (0.1 mg/mL) treatment for 1 h. At end of the time point, culture supernatants were differentially centrifuged at 300 g for 10 min, 2000 g for 20 min and 10,000 g for 30 min to sequentially remove cells, debris, apoptotic bodies and larger microvesicles respectively. The conditioned supernatant was passed through 0.45-μm filter and concentrated using 100 kDa cut-off centrifugal filter units (Amicon). The EVs were precipitated using ExoQuick-TC reagent (System Biosciences) following the manufacturer's instructions and purified from non-EV proteins by repeated washing through 100 kDa cut-off centrifugal filter units. The EVs were resuspended in PBS and stored at −80°C. The EVs were extensively characterized by western blotting against specific markers, electron microscopy, dynamic light scattering and nanoparticle tracking analysis. Individual EV preparations were used for each experiment after normalization with respect to total protein content.

Live-imaging of EV shedding from cells

2 × 10^5 THP-1 cells were labeled with the lipophilic membrane dye, Nile red (40 μg/mL, Invitrogen) and seeded onto poly-lysine coated μ-Slide 8 well chambered slides (Ibidi). The cells were stimulated with 0.5 μg/mL PLY or PBS in an enclosed microscope chamber maintained at 37°C and 5% CO_2. For live-imaging experiments using GFP-tagged PLY (0.4 μg/mL), cells were pre-labelled with Vybrant Dil Cell Labeling solution (1:200; Thermo Fisher Scientific) for 10 min at 37°C. Images were acquired at 5s interval for a total of 20 min under the 63× oil objective of Leica SP8 laser confocal microscope (Leica Microsystems). Videos were processed using the Leica LASX software at 2fps.

Zeta potential and NTA analysis

Zeta potential measurements were performed using the Zetasizer Nano particle analyser (Malvern PANalytical Application lab, Bangalore). Triplicate measurements were performed with standard settings (Refractive Index 1.330, Viscosity 0.8872, Temperature 25°C). The nanoparticle tracking analysis (NTA) was performed using the Nanosight NS300 at Malvern PANalytical Application Lab, Delhi using 20× microscope attached to a CMOS camera. The EVs were diluted in PBS to achieve a minimum of 20 particles per frame and maximum of 120–150 particles per frame.

Immunogold TEM analysis

For transmission electron microscopy, 10 μL of purified EVs was adsorbed onto Formvar coated copper grids (Electron Microscopy Sciences), blocked with 0.1% BSA and incubated with mouse anti-PLY (1:10, Abcam) followed by 12 nm gold conjugated goat anti-mouse IgG (Jackson ImmunoResearch Laboratories) (1:15 dilution). Samples were fixed using 2.5% glutaraldehyde and contrasted using UranyLess stain (Electron Microscopy Sciences). After drying, the grids were observed under the Talos F200i S(TEM) (Thermo Scientific) at 200 kV and 74K magnification.

Immunoblotting for EV markers and PLY

The EVs, 10,000 g pellets and cell pellets were lysed in RIPA lysis buffer and the total protein was quantified and normalized using the Bicinchoninic acid (BCA) protein assay kit (Pierce). The lysates were resolved on 12–15% SDS-PAGE gel and transferred to PVDF membrane. The blots were blocked using 5% BSA for 1 h and probed with mouse anti-CD81 (1:1000, ab79559), rabbit anti-CD63 (1:1000, ab134045), rabbit anti-TSG101 (1:1000, ab125011), mouse anti-Ptx3 (1:500, sc-373951), mouse anti-MOB2 (1:200; sc-81564), rabbit anti-H2BC3 (1:500, PA5-117473), mouse anti-β-actin (1:1000, ab8226), mouse anti-His (1:500, 1706516) and mouse anti-PLY (1:500, ab71810) overnight at 4°C. Precision Plus Protein WesternC standard (Biorad) was used as ladder. HRP-conjugated anti-mouse IgG and anti-rabbit IgG (1:3000, Biorad) were used and imaged using Azure 600 gel imaging system (Azure Biosystems) and iBright FL1500 Imaging system (Invitrogen). Original uncropped blots are shown in Figure S13.

Quantification of PLY in EVs by densitometry

Immunoblotting was performed for EVs with mouse anti-PLY (1:500, ab71810) incubated overnight at 4°C followed by HRP-conjugated anti-mouse IgG (1:3000, Biorad). Blots were imaged using the iBright FL1500 chemidoc system (Invitrogen). PLY level in EVs was quantified by comparing band intensity with recombinant PLY (10–100 ng) loaded as standards after background subtraction and analyzed using ImageJ software version 1.53.

Hemolysis assay

50 μL of the EV suspension in PBS was co-incubated with equal volume of 2% blood suspension in PBS containing 1 mM DTT for 1 h at 37°C in V-shaped bottom 96-well plates (Tarsons). Purified recombinant PLY (0.5 μg/mL and 1 μg/mL) was used as positive control. To control for carry-over of non-EV associated PLY from culture supernatant into the EV preparations, rPLY spiked culture medium was passed through the 100 kDa ultrafiltration spin columns, as performed during EV isolation and the retentate fraction was checked for PLY-hemolytic activity. The plates were centrifuged at 400xg for 15 min and the absorbance of supernatant was measured at 540 nm using the Varioskan LUX multimode microplate reader (Thermo Fisher). Triton X-100 (1%) was used as 100% lysis control and all the values were normalized to this control and relatively expressed as % hemolysis.

PLY-CF647 conjugation and labeling of EVs

Purified recombinant PLY protein was labeled using the Mix-*n*-Stain CF647 labeling kit (1:10, Biotium) for 15 min in dark and the excess dye was removed using 100 kDa MWCO centrifugal spin columns following the manufacturer's protocol. THP-1 monocytes were challenged with CF-674-conjugated PLY and shed EVs were isolated. Isolated EVs were labeled with Nile Red (100 μg/mL) for 30 mins at 37°C and the excess dye was removed using centrifugal spin columns. The Nile Red labeled EVs were incubated for 1 h with DCs cultured on coverslips at 37°C. The cells were fixed with 4% PFA for 10 min and mounted on glass slide using the ProLong Gold anti-fade mounting medium containing DAPI (Invitrogen). Images were acquired under the 63× oil objective of Leica SP8 laser confocal microscope (Leica Microsystems).

CFSE labeling of EVs and DC internalization

EVs were labeled with CFSE dye (10 μM, Invitrogen) for 1 h at 37°C and the excess dye was removed using 100 kDa MWCO centrifugal spin columns. The CFSE labeled EVs were incubated with THP-1 monocyte-derived DCs grown on coverslips for 24 h at 37°C. The cells were fixed with 4% PFA for 10 min and mounted on glass slide using the ProLong Gold anti-fade mounting medium with DAPI (Invitrogen). Images were acquired under the 63× oil objective of Leica SP8 laser confocal microscope (Leica Microsystems).

Mass spectrometry and data analysis

For LC-MS/MS analysis, EVs were isolated as we have described previously in RPMI medium lacking FBS to exclude serum proteins. The EVs were lysed by direct boiling in Rapigest SF (Waters) and relative total protein concentrations normalized to ~1 mg/mL by BCA assay. The samples were reduced using 100 mM 1, 4-Dithiothreitol (Sigma Aldrich), alkylated using 200 mM iodoacetamide (Sigma Aldrich) and digested overnight with MS grade trypsin (Sigma Aldrich) in the ratio 1:25. The injection volume was 2.0 μL and all the samples were injected in duplicate into the nano ACQUITY UPLC chromatographic system (Waters). MS runs were performed using the Synapt G2 High-Definition MS System (Waters). The data was analyzed using the Progenesis QI for Proteomics v4.2 (Non-Linear Dynamics, Waters). Relative protein quantification was performed using the Hi3 label free method. The naive EVs and PLY EVs protein datasets were analyzed with Exocarta and Vesiclepedia databases to distinguish between classical (endoplasmic reticulum/golgi) and non-classical (such as exosomes and microvesicles). The identified protein sets were analyzed for categorization and enrichment levels across functional classifications like KEGG metabolic pathways and Gene Ontology terms. The STRING database within Cytoscape was used to construct a functional protein-protein interaction network to understand the interactions among differentially expressed proteins in PLY EVs. The online tool (http://bioinformatics.psb.ugent.be/webtools/Venn/) was used to visualize the distribution of shared and unique proteins among naive EVs and PLY EVs. The study utilized DESEQ2 in R software to identify and visualize enriched proteins in PLY(0.5) EVs compared to Naive EVs, generating a volcano plot and heatmap. GO enrichment analysis of upregulated genes in PLY EVs was performed using gprofiler (https://biit.cs.ut.ee/gprofiler/gost). The mass spectrometry proteomics data have been deposited to the ProteomeXchange Consortium via the PRIDE[60] partner repository with the dataset identifier PXD052436 and 10.6019/PXD052436.

Flow cytometry of EV uptake and DC maturation

To quantify EV uptake, CFSE-labelled EVs were incubated with 2 × 10^5 DCs for 24 h and the samples were washed and fixed with 4% PFA. The EV uptake was analyzed on the FITC channel using the BD FACS Aria III cytometer (BD Biosciences). For DC maturation assays, immature day 5 stage THP-1 derived DCs were incubated with EVs for 24 h and stained using PE-mouse anti-CD80, Clone L307.4 (BD Biosciences), FITC-Mouse anti-CD86 Clone-2331(BD Biosciences), PE-*anti*-human CD83 clone HB15 (Biolegend) as per manufacturer's instructions. Cells were stained with fixable viability dye (FVD eFluor 780, eBiosciences) to exclude dead cells from analysis. Cells were gated on FVD $^-$ population and analyzed on the BD FACS Aria III cytometer (BD Biosciences). To test whether EV internalization occurs independently of actin-dependent endocytosis, DCs were pretreated with 5 μM cytochalasin D (CytD) for 30 min and co-incubated with Nile-red

labeled EVs for 60 min. Following washes to remove unbound EVs, the percentage of EV-bound DCs was quantified using the BD FACS Aria III cytometer.

The maturation of THP-1 monocyte-derived DCs by PLY-EVs and PLY transfer to recipient cells upon EV addition were validated in primary monocytes isolated from healthy donor blood. Briefly, 3×10^5 primary monocytes were seeded in 12-well plates and co-incubated with Naive EV and PLY-EVs, that were isolated from stimulated THP-1 monocytes (40 μg total EV protein) in DC differentiation medium consisting of RPMI supplemented with 40 ng/mL of human recombinant GM-CSF and IL-4 (Peprotech). As positive control, 40 μg of naive EV was pre-incubated with 0.272 μg of purified PLY protein (6.82 ng/μg EV protein) in accordance with Figure S5D at 37°C for 30 min and then incubated with primary monocytes. At 24 h post incubation with Naive and PLY EVs (80 μg total protein), the cells were washed to remove unbound EVs and lysates were processed for western blotting for detection of PLY using mouse anti-His antibody (Thermo Scientific). At 96 h post-EV challenge, the cells were collected for flow cytometry staining for DC maturation marker, CD83. As positive control for inducing maturation into DCs, monocytes were stimulated with TNF-α (40 ng/mL) and Ionomycin (100 ng/mL) at 72 h post EV stimulation.

Cytokine ELISA

THP- 1 monocyte derived DCs were pre-treated with EVs alone for 24 h and/or subsequently infected with *S. pneumoniae*, T4R for 2 h, followed by removal of extracellular bacteria and incubated for another 24 h. The culture supernatants were analyzed for cytokines using the Human TNF-α and Human IL-12 DuoSet ELISA kits (R&D Systems) following the manufacturer's protocol. The supernatants of BALF from PLY-challenged and infected mice were stored at −80°C for cytokine analysis by mouse TNF-α and IL-1β DuoSet ELISA kits (R&D Systems).

Zebrafish maintenance and EV microinjection

The viable zebrafish eggs were kept in 1X embryo medium 5.03 mM NaCl, 0.17 mM KCl, 0.33 mM $CaCl_2.2H_2O$, 0.33 mM $MgSO4.7H_2O$) at 28.5°C. All microinjection procedures were carried out on 3 days post-fertilization embryos with the help of FemtoJet Microinjector and PatchMan NP2 Micromanipulator (Eppendorf, Germany). Embryos were divided into three groups-mock (E3 embryo medium), Naive EVs (EV), and PLY(0.5) EVs. 60 embryos/group were injected into the duct of Cuvier with 3 nL of the CFSE-labelled EV suspension at a consistent injection time of 0.02 s and 90 hPa pressure. Following the microinjection process, embryos were sorted under a fluorescence microscope (Olympus BX51) and only fluorescence-positive embryos were transferred into the embryo medium and kept in a 28.5°C incubator with constant changing of media at 12 h intervals.

Zebrafish heartbeat, survival and qPCR

Zebrafish embryos were anesthetized using 0.04% Tricaine (Sigma-Aldrich, E10521) for further experimental procedures. Sedated embryos were placed over an agarose mold and heartbeats were assessed manually using an Olympus SZ51 stereomicroscope. The embryos were checked every day, dead larvae were removed and the fraction of surviving larvae was calculated. The experiments were repeated in triplicates. The error bars represent the standard deviation of the survival percentage from the three experiments. The embryos were imaged for four continuous days post-injection using Zeiss 880-Multiphoton confocal microscope. Embryos were anesthetized as stated previously and agar mounted and expression for fluorescence-tagged EVs was measured in three microinjected groups of embryos. Images were processed using ImageJ software.

qPCR experiments were performed using cDNAs prepared from the zebrafish embryos. Amplification of inflammatory cytokine TNF-α (Forward Primer: 5′-GGAGAGTTGCCTTTACCGCT-3′, Reverse Primer: 5′- GATTGCCCTGGGTCTTATGGAG-3′) was carried out with gene-specific exon-exon junction spanning primers using SOLIS BIODYNE HOT FIREPol EvaGreen kit following the manufacturer's protocol. Fluorescence intensities were recorded and analyzed using Qiagen QIAquant 96 5-plex detection machine. Relative mRNA expression was determined by delta delta Ct method, taking into consideration the quantity of target sequences relative to the endogenous control β-actin (Forward Primer: 5′- CACTGAGGCTCCCCTGAATCCC-3′, Reverse Primer: 5′- CGTACAGAGAGAGCACAGCCTGG-3′). Complete information according to the Minimum Information for Publication of Quantitative Real-Time PCR Experiments (MIQE) is shown in Table S1 and Data S1.

Intranasal PLY challenge and EV isolation

6-8 weeks-old wild-type C57BL/6 mice (50% male/female) were anesthetized by inhalation of 4% isofluorane and 50 μL of PBS containing 0.25 μg of recombinant PLY (5 μg/mL) was instilled intranasally into the nostrils. The control group was administered with 50 μL PBS. Mice (≥5/group) were allocated randomly to the control and treated groups. The PLY dose was chosen based on a previous study showing the induction of lung hyperpermeability and acute lung injury in mice upon aerosol administration of PLY.[37] Zafar et al., showed that administration of recombinant PLY dose of 0.2 μg/day induced shedding of pneumococci and mucosal inflammation.[38] Intranasal administration of PLY at 10 ng/g body weight (corresponding to 0.25 μg for 6–8 weeks mice) restored virulence of an avirulent ST306 pneumococcal clone expressing a non-cytolytic PLY variant.[39] Based on the above studies, two intranasal doses of 0.25 and 0.5 μg PLY were tested, but mortality was observed at 0.5 μg dose. Hence, we adopted intranasal dose of 0.25 μg PLY in 50 μL PBS (5 μg/mL) to model PLY-induced acute lung injury. For IVIS imaging experiments, GFP-tagged PLY was administered. To assess lung permeability, 50 μL of 0.5% Evans blue (Sigma) in saline was injected intravenously through the tail vein at 30 min prior to sacrifice as described previously.[61] At 18 h post treatment, mice were sacrificed followed by heart perfusion to drain out blood and the lungs were imaged *ex vivo* for Evans blue dye lung extravasation (Excitation- 620 nm,

Emission- 680 nm) and PLY-GFP (Excitation- 500 nm, Emission- 520 nm) signals in the lungs respectively using the IVIS Spectrum-CT Imaging system (Caliper-Perkin Elmer). Post sacrifice, lungs were perfused with PBS containing 2% FBS and 1 mM EDTA to collect the BALF. The BALF was processed to isolate the cells upon RBC lysis and stained with PE anti-mouse Ly6G clone 1A8 (Biolegend) and FITC anti-mouse F4/80 clone BM8 (Biolegend) for quantification of neutrophils and macrophages by flow cytometry (BD FACS Aria III). The EVs isolated from BALF of PLY and PBS treated mice were administered intranasally to recipient mice at a dose of 18 μg/mouse. EVs were labeled with Nile red dye (100 μg/mL) and excess dye was removed using 100 kDa cut-off centrifugal filter units (Amicon). At 18 h post EV administration, the mice were scored for clinical symptoms and the distribution of Nile-red labeled EVs in mice was imaged using the IVIS system (Excitation- 535 nm, Emission- 620 nm). The infiltration of neutrophils and macrophages in BALF was quantified by flow cytometry. The cell-free supernatant of BALF was stored at −80°C for cytokine analysis by mouse TNF-α and IL-1β DuoSet ELISA kits (R&D Systems). Lungs were perfused with a 1:1 mixture of OCT and 4% PFA and preserved in OCT cryomolds (Tissue-Tek) at −80°C. 10 μm sections were sectioned using the cryotome (CM1850UV Leica) and embedded in poly-l-lysine coated slides for H&E staining. Images were acquired through Olympus CKX53 Microscope under the 10× objective.

Mouse infection and adoptive transfer of EVs

6-8 weeks old male wild-type C57BL/6 mice were sedated by inhalation of 4% isofluorane and 50 μL of PBS containing 4×10^6 CFU of wild-type T4 or the isogenic PLY mutant strain, T4Δply was administered into the nares. Control group was administered with 50 μL of sterile PBS. Mice (≥5/group) were allocated randomly to the control and treatment groups. The mice were monitored and scored for clinical symptoms twice a day. At day 4 post infection, mice were sacrificed and BALF was collected after draining out blood by heart perfusion. Bacterial counts were determined from BALF by viable count on blood agar plates. The EVs were isolated from BALF as described earlier and normalized for total protein content using BCA assay. The EVs were labeled with Nile-red and administered to recipient mice at a dose of 35 μg/mice. The dose was calculated based on the EV quantity obtained from BALF collected from single mice. At 18 h, the EV distribution in mice was imaged using the IVIS system. The mice were sacrificed and the infiltration of neutrophils and macrophages in BALF was quantified by flow cytometry. The cytokine, TNF-α in mouse BALF supernatant was measured by DuoSet ELISA kit (R&D Systems). 10 μm lungs tissue sections were subjected to H&E staining. Images were acquired through Olympus CKX53 Microscope under the 10× objective.

QUANTIFICATION AND STATISTICAL ANALYSIS

Data were statistically analyzed using GraphPad Prism v.9.1.2. Data represent mean ± SEM unless otherwise specified. Experiments were performed with three biological replicates with triplicates. The exact N numbers (biological replicates) are indicated in the respective figure legends. Pairwise comparison of normalized data was analyzed using unpaired t-tests. Comparison between multiple groups was performed using one-way or two-way ANOVA as appropriate followed by Tukey's or Bonferroni's multiple comparison post-hoc tests as indicated. Differences were considered significant at $*p < 0.05$, $**p < 0.01$; $***p < 0.001$, $****p < 0.0001$, NS denotes not significant.